

Response to editor comments

Dear Dr. Kaiser,

Thank you for your suggestions. I think I misunderstood some of your previous comments so there are some unclear expressions. Thank you for pointing them out, we have fixed them, which definitely improved the quality of our calculations as well as this manuscript.

For the supplementary information file, I did not upload anything in the last round. However, it seems that if we do not upload new file to overwrite the current supplementary file, it would remain unchanged and we cannot delete this file. Thus, in this draft I will upload a blank page to overwrite the current file, and if anything goes wrong, I will contact the editorial office to clarifying this problem.

In the meantime, I would like to point out that we spotted a calculation error in the previous manuscript. When calculating the EIE factor using the equations without approximation, I made a mistake when calculating $(1+\delta(\text{NO}_2))$. The $1+\delta(\text{NO}_2)$ values in our experiments should range from 0.948 to 0.956 but I accidentally made it 0.9948 to 0.9956. After fixing this mistake, we see the linear trend became more robust (R^2 increased from 0.96 to 0.9975) and the slope changed from 26.8‰ to 28.1‰. As a result, the EIE value became 28.9‰ instead of 27.5‰. We have revised this number throughout the manuscript. However, this change of 1.4‰ did not affect our entire story or the following LCIE calculations.

We re-calculated the LCIE using the equations without approximations after we changed the EIE value. The calculated LCIE value remain the same. Additionally, in order to show the consistency of the equations and the links between Fig. 1B and C, we revised Fig. 1B, C to better compare the two sets of data.

Additionally, I have added a table (Table 1) in the text to display all the data. However, I would like to mention that I deposited this data to the “open science framework” following the requirement on ACP website before we submitted the manuscript last year (please refer to the ‘data availability’ section in the end of the manuscript). The deposited data is almost the same as table 1, I hope it is OK.

Please see below for a point-by point response to your comments:

I noticed that you have now re-cast Eq. 8 as a function of three delta values, $\delta(\text{NO})$, $\delta(\text{NO}_2)$ and $\delta(\text{NO}_x)$. This does not make sense because in your calculations in the Appendix, you are trying to eliminate one of the three unknowns using mass balance. Since you measure $\delta(\text{NO}_2)$ and assume that $\delta(\text{NO}_x)$ is constant, it would seem to make sense to cast the equations 8 (or 7) in terms of $\delta(\text{NO}_2)$ and $\delta(\text{NO}_x)$ – as you did in fact in the previous version of the manuscript. This also helps makes the link back to equation 3 and the link between Figs. 1B and 1C. I would therefore suggest you keep the previous version (using just the measured values, i.e. $\delta(\text{NO}_2)$ and $\delta(\text{NO}_x)$), with the corrections I pointed out before and make the axes of Figs. 1B and 1C consistent with equations 3 and a version of Eq. 8 using just these two variables, i.e.

$$\delta_2 - \delta_x = (1 + \delta_2)[1 - f(\text{NO}_2)] \frac{(\alpha_2 - \alpha_1)A + \varepsilon}{1 + A\alpha_2 + \varepsilon}$$

or (better)

$$\frac{\delta_2 - \delta}{1 + \delta_2} = \frac{1}{1 - f(\text{NO}_2)} \frac{\delta_2 - \delta_x}{1 + \delta_2} = \frac{(\alpha_2 - \alpha_1)A + \varepsilon}{1 + A\alpha_2 + \varepsilon}$$

This last version might be the most convenient because it explicitly shows the link between the y-axis label of Fig. 1C (slight recast from the version currently in the paper) and the conversion relation between the measured and the plotted values.

I am still not convinced that the approximation you are making ($1 + A\alpha_1 = 1 + A$) is necessary, convenient, or otherwise helpful. Actually, for large A (which prevail at Summit, 1. 409), the approximation you are making changes the asymptotic behavior of Eqs. 7 (and 8), which should be correctly

$$\lim_{A \rightarrow \infty} \frac{\delta_2 - \delta}{1 + \delta_2} = \frac{\alpha_2 - \alpha_1}{\alpha_2}$$

rather than

$$\lim_{A \rightarrow \infty} \frac{\delta_2 - \delta}{1 + \delta_2} = \alpha_2 - \alpha_1$$

In any case, the approximation is not necessary because you have to make assumptions about the magnitude of α_2 . Of course, you are right that the correction is small, but this is often the case for δ values and these small non-linearities are just due to the way δ values (relative isotope ratio differences) are defined. The approximations might have had their place when people were still doing calculations by hand (or maybe pocket calculator), but they don't really have any justification when everyone uses a computer. It would also simplify the paper if you removed the approximation (fewer equations and verbal explanation required). However, if you wanted to retain it, please give the correct solution and make it explicit what difference it makes when the approximation is applied, e.g. by writing Eqs. 7/8 as follows (using the correct approximation symbol \approx , not \sim):

$$\frac{\delta_2 - \delta}{1 + \delta_2} = \frac{1}{1 - f(\text{NO}_2)} \frac{\delta_2 - \delta_x}{1 + \delta_2} = \frac{(\alpha_2 - \alpha_1)A + \varepsilon}{1 + A\alpha_2 + \varepsilon} \approx \frac{(\alpha_2 - \alpha_1)A + \varepsilon}{1 + A}$$

We agree that we should use $\delta(\text{NO}_2)$, $\delta(\text{NO}_x)$ instead of $\delta(\text{NO})$ in the figure, because these are the values we measured. We have revised the equations according to the calculation above and now we only used the measured values to plot Figure 1B and C. In the meantime, we provided

both accurate calculation as well as approximation in Eq. 7 and 8. Figures 1 and 2 are also revised **using the equations without approximations**.

l. 136 & 155: Please use the correct approximation symbol \approx (double wavy lines; not \sim , which has other mathematical meanings).

Revised as suggested.

l. 113, 114 & 139: Please replace "ppb" with the SI unit "nmol mol⁻¹".

Revised as suggested.

l. 193: You mention that the method description includes three experiments that measured $\delta(\text{NO}_x)$, but the methods only refer to measurements of $\delta(\text{NO}_2)$. Are these the experiments when you titrate O₃ with NO? Please clarify this.

Thank you for pointing this out. In the previous version of the manuscript, we mentioned the measurement of $\delta(\text{NO}_x)$ after we discussed the setup of two sets of experiments. To clarify this question, we moved this description up and made it a new paragraph (lines 121-126 in the manuscript).

Finally, I noticed that a table is missing showing the experimental conditions and explicit results, which is required as per the journal's data policy. Please add such a table with a list of the 13 (?) experiments including initial and final NO, NO₂ and O₃ mole fractions, calculated $f(\text{NO}_2)$ values as well as the measured $\delta(\text{NO}_2)$ values.

We added a table (Table 1) in the manuscript after the figures. In the discussion, we referred to the table when discussing the results of our experiments.

List of changes

1. Equations 7 and 8 were revised to show the non-approximated equations as well as an approximated expression. The figures are also re-plotted to show the non-approximated results.
2. We fixed a previous miscalculation of the EIE value, which changed the EIE value from 1.0275 to 1.0289.
3. A table showing all the results is added.
4. Symbol ' \sim ' was replaced by ' \approx ', unit 'ppb' was replaced by ' nmol mol^{-1} '.

1 **Quantifying the nitrogen isotope effects during photochemical**
2 **equilibrium between NO and NO₂: implications for δ¹⁵N in**
3 **tropospheric reactive nitrogen**

4 Jianghanyang Li¹, Xuan Zhang², John Orlando², Geoffrey Tyndall² and Greg Michalski^{1,3}

5 ¹. Department of Earth, Atmospheric and Planetary Sciences, Purdue University, West Lafayette,
6 IN, 47907

7 ². Atmospheric Chemistry Observations and Modeling Lab, National Center for Atmospheric
8 Research, Boulder, CO, 80301

9 ³. Department of Chemistry, Purdue University, West Lafayette, IN, 47907

10 *Correspondence to:* Jianghanyang Li (li2502@purdue.edu)

11 **Abstract.** Nitrogen isotope fractionations between nitrogen oxides (NO and NO₂) play a
12 significant role in determining the nitrogen isotopic compositions (δ¹⁵N) of atmospheric reactive
13 nitrogen. Both the equilibrium isotopic exchange between NO and NO₂ molecules and the isotope
14 effects occurring during the NO_x photochemical cycle are important, but both are not well
15 constrained. The nighttime and daytime isotopic fractionations between NO and NO₂ in an
16 atmospheric simulation chamber at atmospherically relevant NO_x levels were measured. Then, the
17 impact of NO_x level and NO₂ photolysis rate to the combined isotopic fractionation (equilibrium
18 isotopic exchange and photochemical cycle) between NO and NO₂ were calculated. It was found
19 that the isotope effects occurring during the NO_x photochemical cycle can be described using a
20 single fractionation factor, designated the Leighton Cycle Isotope Effect (LCIE). The results
21 showed that at room temperature, the fractionation factor of nitrogen isotopic exchange is
22 1.0289±0.0019, and the fractionation factor of LCIE (when O₃ solely controls the oxidation from
23 NO to NO₂) is 0.990±0.005. The measured LCIE factor showed good agreement with previous
24 field measurements, suggesting that it could be applied in ambient environment, although future
25 work is needed to assess the isotopic fractionation factors of NO + RO₂/HO₂ → NO₂. The results
26 were used to model the NO-NO₂ isotopic fractionations under several NO_x conditions. The model
27 suggested that isotopic exchange was the dominate factor when NO_x >20 nmol mol⁻¹, while LCIE
28 was more important at low NO_x concentrations (<1 nmol mol⁻¹) and high rates of NO₂ photolysis.
29 These findings provided a useful tool to quantify the isotopic fractionations between tropospheric
30 NO and NO₂, which can be applied in future field observations and atmospheric chemistry models.
31

Deleted: 0275

Deleted: 0012

32

35 **1. Introduction**

36 The nitrogen isotopic composition ($\delta^{15}\text{N}$) of reactive nitrogen compounds in the
37 atmosphere is an important tool in understanding the sources and chemistry of atmospheric NO_x
38 ($\text{NO}+\text{NO}_2$). It has been suggested that the $\delta^{15}\text{N}$ value of atmospheric nitrate (HNO_3 , nitrate
39 aerosols and nitrate ions in the precipitation and snow) imprints the $\delta^{15}\text{N}$ value of NO_x sources
40 (Elliott et al., 2009; Kendall et al., 2007) thus many studies have used the $\delta^{15}\text{N}$ values of
41 atmospheric nitrate to investigate NO_x sources (Chang et al., 2018; Felix et al., 2012; Felix &
42 Elliott, 2014; Gobel et al., 2013; Hastings et al., 2004, 2009; Morin et al., 2009; Park et al., 2018;
43 Walters et al., 2015, 2018). However, there remain questions about how isotopic fractionations
44 that may occur during photochemical cycling of NO_x could alter the $\delta^{15}\text{N}$ values as it partitions
45 into NO_y (NO_y = atmospheric nitrate, NO_3 , N_2O_5 , HONO , etc., Chang et al., 2018; Freyer, 1991;
46 Hastings et al., 2004; Jarvis et al., 2008; Michalski et al., 2005; Morin et al., 2009; Zong et al.,
47 2017). Similarly, other complex reactive nitrogen chemistry, such as nitrate photolysis and re-
48 deposition in ice and snow (Frey et al., 2009), may impact the $\delta^{15}\text{N}$ of NO_y and atmospheric nitrate.
49 The fractionation between NO and NO_2 via isotope exchange has been suggested to be the
50 dominant factor in determining the $\delta^{15}\text{N}$ of NO_2 and ultimately atmospheric nitrate (Freyer, 1991;
51 Freyer et al., 1993; Savarino et al., 2013; Walters et al., 2016). However, isotopic fractionations
52 occur in most, if not all, NO_x and NO_y reactions, while most of these are still unknown or, if
53 calculated (Walters and Michalski, 2015), unverified by experiments. Since the atmospheric
54 chemistry of NO_y varies significantly in different environments (e.g., polluted vs. pristine, night
55 vs. day), the isotopic fractionations associated with NO_y chemistry are also likely to vary in
56 different environments. These unknowns could potentially bias conclusions about NO_x source
57 apportionment reached when using nitrogen isotopes. Therefore, understanding the isotopic

58 fractionations between NO and NO₂ during photochemical cycling could improve our
59 understanding of the relative role of sources versus chemistry for controlling the δ¹⁵N variations
60 of atmospheric NO₂ and nitrate.

61 In general, there are three types of isotopic fractionation effects associated with NO_x
62 chemistry (Fig. 1A). The first type is the equilibrium isotopic effect (EIE), i.e., isotope exchange
63 between two compounds without forming new molecules (Urey, 1947, Bigeleisen and Mayer,
64 1947), which for nitrogen isotopes in the NO_x system is the $^{15}\text{NO} + ^{14}\text{NO}_2 \leftrightarrow ^{14}\text{NO} + ^{15}\text{NO}_2$
65 exchange reaction (Begun and Melton, 1956, Walters et al., 2016). The second type is the kinetic
66 isotopic effect (KIE) associated with difference in isotopologue rate coefficients during
67 unidirectional reactions (Bigeleisen & Wolfsberg, 1957). In the NO_x system this KIE would
68 manifest in the oxidation of NO into NO₂ by O₃/HO₂/RO₂. The third type is the photochemical
69 isotope fractionation effect (PHIFE, Miller & Yung, 2000), which for NO_x is the isotopic
70 fractionation associated with NO₂ photolysis. All three fractionations could impact the δ¹⁵N value
71 of NO₂, and consequently atmospheric nitrate, but the relative importance of each may vary.

72 The limited number of studies on the EIE in the NO_x cycle have significant uncertainties.
73 Discrepancies in the EIE for $^{15}\text{NO} + ^{14}\text{NO}_2 \leftrightarrow ^{14}\text{NO} + ^{15}\text{NO}_2$ have been noted in several studies.
74 Theoretical calculations predicted isotope fractionation factors (α) ranging from 1.035 to 1.042 at
75 room temperature (Begun & Fletcher, 1960; Monse et al., 1969; Walters & Michalski, 2015) due
76 to the different approximations used to calculate harmonic frequencies in each study. Likewise,
77 two separate experiments measured different room temperature fractionation factors of
78 1.028 ± 0.002 (Begun & Melton, 1956) and 1.0356 ± 0.0015 (Walters et al., 2016). A concern in both
79 experiments is that they were conducted in small chambers with high NO_x concentrations
80 (hundreds of μmol mol⁻¹), significantly higher than typical ambient atmospheric NO_x levels

81 (usually less than $0.1 \mu\text{mol mol}^{-1}$). Whether the isotopic fractionation factors determined by these
82 experiments are applicable in the ambient environment is uncertain because of possible wall effects
83 and formation of higher oxides, notably N_2O_4 and N_2O_3 at these high NO_x concentrations.

84 Even less research has examined the KIE and PHIFE occurring during NO_x cycling. The
85 KIE of $\text{NO} + \text{O}_3$ has been theoretically calculated (Walters and Michalski, 2016) but has not been
86 experimentally verified. The NO_2 PHIFE has not been experimentally determined or theoretically
87 calculated. As a result, field observation studies often overlook the effects of PHIFE and KIE.
88 Freyer et al. (1993) measured NO_x concentrations and the $\delta^{15}\text{N}$ values of NO_2 over a 1-year period
89 at Jülich, Germany and inferred a combined NO_x isotope fractionation factor (EIE+KIE+PHIFE)
90 of 1.018 ± 0.001 . Freyer et al. (1993) suggested that the NO_x photochemical cycle (KIE and PHIFE)
91 tends to diminish the equilibrium isotopic fractionation (EIE) between NO and NO_2 . Even if this
92 approach were valid, applying this single fractionation factor elsewhere, where NO_x , O_3
93 concentrations and actinic fluxes are different, would be tenuous given that these factors may
94 influence the relative importance of EIE, KIE and PHIFE (Hastings et al., 2004; Walters et al.,
95 2016). Therefore, to quantify the overall isotopic fractionations between NO and NO_2 at various
96 tropospheric conditions, it is crucial to know 1) isotopic fractionation factors of EIE, KIE and
97 PHIFE individually and 2) the relative importance of each factor under various conditions.

98 In this work, we aim to quantify the nitrogen isotope fractionation factors between NO and
99 NO_2 at photochemical equilibrium. First, we measure the N isotope fractionations between NO
100 and NO_2 in an atmospheric simulation chamber at atmospherically relevant NO_x levels. Then, we
101 provide mathematical solutions to assess the impact of NO_x level and NO_2 photolysis rate ($j(\text{NO}_2)$)
102 to the relative importance of EIE, KIE and PHIFE. Subsequently we use the solutions and chamber
103 measurements to calculate the isotopic fractionation factors of EIE, KIE and PHIFE. Lastly, using

104 the calculated fractionation factors and the equations, we model the NO-NO₂ isotopic
105 fractionations at several sites to illustrate the behavior of δ¹⁵N values of NO_x in the ambient
106 environment.

107

108 2. Methods

109 The experiments were conducted using a 10 m³ Atmospheric Simulation Chamber at the
110 National Center for Atmospheric Research (see descriptions in Appendix A and Zhang et al.
111 (2018)). A set of mass flow controllers was used to inject NO and O₃ into the chamber. NO was
112 injected at 1 L min⁻¹ from an in-house NO/N₂ cylinder (133.16 μmol mol⁻¹ NO in ultra-pure N₂),
113 and O₃ was generated by flowing 5 L min⁻¹ zero-air through a flow tube equipped with a UV Pen-
114 Ray lamp (UVP LLC., CA) into the chamber. NO and NO₂ concentrations were monitored in real
115 time by chemiluminescence with a detection limit of 0.5 ~~nmol mol⁻¹~~ (model CLD 88Y, Eco Physics,
116 MI) as were O₃ concentrations using an UV absorption spectroscopy with a detection limit of 0.5
117 ~~nmol mol⁻¹~~ (model 49, Thermo Scientific, CO). In each experiment, the actual amounts of NO and
118 O₃ injected were calculated using measured NO_x and O₃ concentrations after steady state was
119 reached (usually within 1 h). The wall loss rate of NO₂ was tested by monitoring O₃ (29 nmol mol⁻¹
120 ¹) and NO_x (62 nmol mol⁻¹) over a 4-hour period. After the NO and NO₂ concentrations reached
121 steady state, no decrease in NO₂ concentrations was observed showing that chamber wall loss was
122 negligible.

123 Three experiments were conducted to measure the δ¹⁵N value of the tank NO (i.e., the δ¹⁵N
124 value of total NO_x). In each of these experiments, a certain amount of O₃ was first injected into the
125 chamber, then approximately the same amount of NO was injected into the chamber to ensure 100%
126 of the NO_x was in the form of NO₂ with little O₃ (<15 nmol mol⁻¹) remaining in the chamber, such

Deleted: ppb

Deleted: ppb

129 ~~that the O₃+NO₂ reaction was negligible. The NO₂ in the chamber was then collected and its δ¹⁵N~~
130 ~~value measured, which equates to the δ¹⁵N value of the tank NO.~~

Moved (insertion) [1]

Deleted: →

131 Two sets of experiments were conducted to separately investigate the EIE, KIE and PHIFE.
132 The first set of experiments was conducted in the dark. In each of these dark experiments, a range
133 of NO and O₃ ([O₃] < [NO]) was injected into the chamber to produce NO-NO₂ mixtures with
134 [NO]/[NO₂] ratios ranging from 0.43 to 1.17. The N isotopes of these mixtures were used to
135 investigate the EIE between NO and NO₂. The second set of experiments was conducted under
136 irradiation of UV lights (300-500 nm, see Appendix A for irradiation spectrum). Under such
137 conditions, NO, NO₂ and O₃ reached photochemical steady state, which combined the isotopic
138 effects of EIE, KIE and PHIFE.

Formatted: Indent: First line: 0.5"

139 In all experiments, the concentrations of NO, NO₂ and O₃ were allowed to reach steady
140 state, and the product NO₂ was collected from the chamber using a honeycomb denuder tube. After
141 the NO, NO₂ and O₃ concentrations reached steady-state, well-mixed chamber air was drawn out
142 through a 40 cm long Norprene Thermoplastic tubing at 10 L min⁻¹ and passed through a
143 honeycomb denuder system (Chemcomb 3500, Thermo Scientific). Based on flow rate, the NO₂
144 residence time in the was less than 0.5 second, thus in the light-on experiments where NO and O₃
145 coexisted, the NO₂ produced inside the transfer tube through NO+O₃ reactions should be <0.03
146 nmol mol⁻¹ (using the upper limit of NO and O₃ concentrations in our experiments). The

Deleted: In addition, three experiments were conducted to measure the δ¹⁵N value of the tank NO. In each of these experiments, a certain amount of O₃ was first injected into the chamber, then approximately the same amount of NO was injected into the chamber to ensure 100% of the NO_x was in the form of NO₂ with little O₃ (<3 nmol mol⁻¹) remaining in the chamber, such that the O₃+NO₂ reaction was negligible.

Moved up [1]: The NO₂ in the chamber was then collected and its δ¹⁵N value measured, which equates to the δ¹⁵N value of the tank NO.

Deleted: ~40 cm

147 honeycomb denuder system consisted of two honeycomb denuder tubes connected in series. Each
148 honeycomb denuder tube is a glass cylinder of 38 mm long, 47 mm in diameter, and consist of 212
149 hexagonal tubes with inner diameters of 2 mm. Before collecting samples, each denuder tube was
150 coated with a solution of 10% KOH and 25% guaiacol in methanol and then dried by flowing N₂
151 gas through the denuder tube for 15 seconds (Williams and Grosjean, 1990, Walters et al., 2016).

Deleted: ppb

166 The NO_2 reacted with guaiacol coating and was converted into NO_2^- that was retained on the
167 denuder tube wall (Williams and Grosjean, 1990). NO was inert to the denuder tube coating: a
168 control experiment sampled pure NO using the denuder tubes, which did not show any measurable
169 NO_2^- . The NO_2 collection efficiency of a single honeycomb denuder tube was tested in another
170 control experiment: air containing 66 nmol mol^{-1} of NO_2 was drawn out of the chamber through a
171 denuder tube, and the NO_2 concentration at the exit of the tube holder was measured and found to
172 be below the detection limit ($<1 \text{ nmol mol}^{-1}$), suggesting the collection efficiency was nearly 100%
173 when $[\text{NO}_2] < 66 \text{ nmol mol}^{-1}$. Furthermore, when the denuder system consisted of two denuder
174 tubes in series and NO_2^- in the second denuder was below the detection limit indicating trivial NO_2
175 breakthrough. Each NO_2 collection lasted for 0.5-3 hours in order to collect enough NO_2^- for
176 isotopic analysis (at least 300 nmol). After collection, the NO_2^- was leached from each denuder
177 tube by rinsing thoroughly with 10 ml deionized water into a clean polypropylene container and
178 stored frozen until isotopic analysis. Isotopic analysis was conducted at Purdue Stable Isotope
179 Laboratory. For each sample, approximately 50 nmol of the NO_2^- extract was mixed with 2 M
180 sodium azide solution in acetic acid buffer in an air-tight glass vial, then shaken overnight to
181 completely reduce all the NO_2^- to $\text{N}_2\text{O}_{(\text{g})}$ (Casciotti & McIlvin, 2007; McIlvin & Altabet, 2005).
182 The product N_2O was directed into a Thermo GasBench equipped with cryo-trap, then the $\delta^{15}\text{N}$ of
183 the N_2O was measured using a Delta-V Isotope Ratios Mass Spectrometer. Six coated denuders
184 tubes that did not get exposed to NO_2 were also analyzed using the same chemical procedure,
185 which did not show any measurable signal on the IRMS, suggesting the blank from both sampling
186 process and the chemical conversion process was negligible. The overall analytical uncertainty for
187 $\delta^{15}\text{N}$ analysis was 0.5 ‰ (1σ) based on replicate analysis of in house NO_2^- standards.

188

Deleted: (~

190 3. Results and Discussions

191 3.1. Equilibrium Isotopic Fractionation between NO and NO₂

192 The equilibrium isotope fractionation factor, $\alpha(\text{NO}_2\text{-NO})$, is the ¹⁵N enrichment in NO₂
193 relative to NO, and is expressed as the ratio of rate constants k_2 / k_1 of two reactions:



196 where k_1 is the rate constant of the isotopic exchange, which was previously determined to be
197 $8.14 \times 10^{-14} \text{ cm}^3 \text{ s}^{-1}$ (Sharma et al., 1970). The reaction time required for NO-NO₂ to reach isotopic
198 equilibrium was estimated using the exchange rate constants in a simple kinetics box model
199 (BOXMOX, Knote et al., 2015). The model predicts that at typical NO_x concentrations used during
200 the chamber experiments ($7.7\text{-}62.4 \text{ nmol mol}^{-1}$), isotopic equilibrium would be reached within 15
201 minutes (see Appendix B). Since the sample collection usually started 1 hour after NO_x was well
202 mixed in the chamber, there was sufficient time to reach full isotope equilibrium. The isotope
203 equilibrium fractionation factor ($\alpha(\text{NO}_2\text{-NO})$) is then calculated to be:

204
$$\alpha(\text{NO}_2 - \text{NO}) = \frac{[^{15}\text{NO}_2][^{14}\text{NO}]}{[^{14}\text{NO}_2][^{15}\text{NO}]} = \frac{R(\text{NO}_2)}{R(\text{NO})}$$
 Eq. (1)

205 where $R(\text{NO}, \text{NO}_2)$ are the ¹⁵N/¹⁴N ratios of NO and NO₂. By definition, the
206 $\delta^{15}\text{N}(\text{NO}) = (R(\text{NO})/R(\text{reference}) - 1) \times 1000 \text{ ‰}$ and $\delta^{15}\text{N}(\text{NO}_2) = (R(\text{NO}_2)/R(\text{reference}) - 1) \times 1000 \text{ ‰}$,
207 but hereafter, the $\delta^{15}\text{N}$ values of NO, NO₂ and NO_x will be referred as $\delta(\text{NO})$, $\delta(\text{NO}_2)$ and $\delta(\text{NO}_x)$,
208 respectively. Eq. (1) leads to:

209
$$\delta(\text{NO}_2) - \delta(\text{NO}) = (\alpha(\text{NO}_2 - \text{NO}) - 1) (1 + \delta(\text{NO}))$$
 Eq. (2)

210 Using Eq. (2) and applying NO_x isotopic mass balance ($\delta(\text{NO}_x) = f(\text{NO}_2)\delta(\text{NO}_2) + (1 - f(\text{NO}_2))\delta(\text{NO})$),
211 $f(\text{NO}_2) = [\text{NO}_2] / ([\text{NO}] + [\text{NO}_2])$ yields:

212
$$\frac{\delta(\text{NO}_2) - \delta(\text{NO}_x)}{1 + \delta(\text{NO}_2)} = \frac{\alpha(\text{NO}_2\text{-NO}) - 1}{\alpha(\text{NO}_2\text{-NO})} (1 - f(\text{NO}_2))$$
 Eq. (3)

213 Here, $\delta(\text{NO}_x)$ equals to the $\delta^{15}\text{N}$ value of the cylinder NO and $f(\text{NO}_2)$ is the molar fraction of NO_2
214 with respect to total NO_x . Three experiments (Table 1) that measured $\delta(\text{NO}_x)$ showed consistent
215 $\delta(\text{NO}_x)$ values of $(-58.7 \pm 0.8) \text{‰}$ ($n = 3$), indicating $\delta(\text{NO}_x)$ remained unchanged throughout the
216 experiments (as expected for isotope mass balance). Thus, the $\delta(\text{NO}_x)$ can be treated as a constant
217 in Eq. (3), and the linear regression of $(\delta(\text{NO}_2) - \delta(\text{NO}_x)) / (1 + \delta(\text{NO}_2))$ versus $1 - f(\text{NO}_2)$ should have
218 an intercept of 0 and a slope of $(\alpha(\text{NO}_2\text{-NO}) - 1) / \alpha(\text{NO}_2\text{-NO})$.

219 The plot of $(\delta(\text{NO}_2) - \delta(\text{NO}_x)) / (1 + \delta(\text{NO}_2))$ as a function of $1 - f(\text{NO}_2)$ values from five
220 experiments yields an $\alpha(\text{NO}_2\text{-NO})$ value of 1.0289 ± 0.0019 at room temperature (Fig. 1B and Table
221 1). This fractionation factor is comparable to previously measured values but with some
222 differences. Our result agrees well with the $\alpha(\text{NO}_2\text{-NO})$ value of 1.028 ± 0.002 obtained by Begun
223 and Melton (1956) at room temperature. However, Walters et al., (2016) determined the $\alpha(\text{NO}_2\text{-}$
224 $\text{NO})$ values of NO- NO_2 exchange in a 1-liter reaction vessel, which showed a slightly higher
225 $\alpha(\text{NO}_2\text{-NO})$ value of 1.035. This discrepancy might originate from rapid heterogeneous reactions
226 on the wall of the reaction vessel at high NO_x concentrations and the small chamber size used by
227 Walters et al. (2016). They used a reaction vessel made of Pyrex, which is known to absorb water
228 (Do Remus et al., 1983; Takei et al., 1997) that can react with NO_2 forming HONO, HNO_3 and
229 other N compounds. Additionally, previous studies have suggested that Pyrex walls enhance the
230 formation rate of N_2O_4 by over an order of magnitude (Barney & Finlayson-Pitts, 2000; Saliba et
231 al., 2001), which at isotopic equilibrium is enriched in ^{15}N compared to NO and NO_2 (Walters &
232 Michalski, 2015). Therefore, their measured $\alpha(\text{NO}_2\text{-NO})$ might be slightly higher than the actual
233 $\alpha(\text{NO}_2\text{-NO})$ value. In this work, the 10 m^3 chamber has a much smaller surface to volume ratio
234 relative to Walters et al. (2016) which minimizes wall effects, and the walls were made of Teflon
235 that minimize NO_2 surface reactivity, which was evidenced by the NO_2 wall loss control

Deleted: see descriptions in method section

Deleted: 0275

Deleted: 0012

239 experiment. Furthermore, the low NO_x mixing ratios in our experiments minimized N₂O₄ and N₂O₃
240 formation. At NO and NO₂ concentrations of 50 nmol mol⁻¹ the steady state concentrations of N₂O₄
241 and N₂O₃ were calculated to be 0.014 and 0.001 pmol mol⁻¹, respectively (Atkinson et al., 2004).

242 Therefore, we suggest our measured $\alpha(\text{NO}_2\text{-NO})$ value (1.0289 ± 0.0019) may better reflect the
243 room temperature (298 K) NO-NO₂ EIE in the ambient environment.

244 Unfortunately, the chamber temperature could not be controlled so we were not able to
245 investigate the temperature dependence of the EIE. Hence, we speculate that the $\alpha(\text{NO}_2\text{-NO})$
246 follows a similar temperature dependence pattern calculated in Walters et al. (2016). Walters et al.
247 (2016) suggested that, the $\alpha(\text{NO}_2\text{-NO})$ value would be 0.0047 higher at 273 K and 0.002 lower at
248 310 K, relative to room temperature (298 K). Using this pattern and our experimentally determined

249 data, we suggest the $\alpha(\text{NO}_2\text{-NO})$ values at 273 K, 298 K and 310 K are 1.0336 ± 0.0019 ,
250 1.0289 ± 0.0019 and 1.0269 ± 0.0019 , respectively. This 0.0067 variation at least partially contribute
251 to the daily and seasonal variations of $\delta^{15}\text{N}$ values of NO₂ and nitrate in some areas (e.g., polar
252 regions with strong seasonal temperature variation). Thus, future investigations should be
253 conducted to verify the EIE temperature dependence.

254

255 3.2. Kinetic isotopic fractionation of Leighton Cycle

256 The photochemical reactions of NO_x will compete with the isotope exchange fractionations
257 between NO and NO₂. The NO-NO₂ photochemical cycle in the chamber was controlled by the
258 Leighton cycle: NO₂ photolysis and the NO + O₃ reaction. This is because there were no VOCs in
259 the chamber so no RO₂ was produced, which excludes the NO + RO₂ reaction. Likewise, the low
260 water vapor content (RH<10%) and the minor flux of photons < 310 nm results in minimal OH
261 production and hence little HO₂ formation and subsequently trivial amount of NO₂ would be

Deleted: 0275

Deleted: 0012

Deleted: 0322

Deleted: 0012

Deleted: 0275

Deleted: 0012

Deleted: 0255

Deleted: 0012

270 formed by NO + HO₂. Applying these limiting assumptions, the EIE between NO and NO₂ (R1-
 271 R2) were only competing with the KIE (R3-R4) and the PHIFE in R5-R6:



276 In which $j(\text{NO}_2)$ is the NO₂ photolysis rate ($1.4 \times 10^{-3} \text{ s}^{-1}$ in these experiments), k_5 is the rate constant
 277 for the NO+O₃ reaction ($1.73 \times 10^{-14} \text{ cm}^3 \text{ s}^{-1}$, Atkinson et al., 2004), and $\alpha_{1,2}$ are isotopic
 278 fractionation factors for the two reactions. Previous studies (Freyer et al., 1993; Walters et al.,
 279 2016) have attempted to assess the competition between EIE (R1-R2), KIE and PHIFE (R3-R6),
 280 but none of them quantified the relative importance of the two processes, nor were α_1 or α_2 values
 281 experimentally determined. Here we provide the mathematical solution of EIE, KIE and PHIFE to
 282 illustrate how R1-R6 affect the isotopic fractionations between NO and NO₂.

283 First, the NO₂ lifetime with respect to isotopic exchange with NO (τ_{exchange}) and photolysis
 284 (τ_{photo}) was determined:

285
$$\tau_{\text{exchange}} = \frac{1}{k_1 [\text{NO}]}$$
 Eq. (4)

286
$$\tau_{\text{photo}} = \frac{1}{j(\text{NO}_2)}$$
 Eq. (5)

287 We then define an A factor:

288
$$A = \begin{cases} \frac{\tau_{\text{exchange}}}{\tau_{\text{photo}}} & \text{when } j(\text{NO}_2) \neq 0 \\ 0 & \text{when } j(\text{NO}_2) = 0 \end{cases}$$
 Eq. (6)

289 Using R1-R6 and Eq. (1)-(6), we solved steady-state $\delta(\text{NO}_2)$ and $\delta(\text{NO})$ values (see calculations
 290 in Appendix C). Our calculations show that the $\delta(\text{NO}_2)$ - $\delta(\text{NO})$ and $\delta(\text{NO}_2)$ - $\delta(\text{NO}_x)$ values at steady
 291 state can be expressed as functions of α_1 , α_2 , $\alpha(\text{NO}_2\text{-NO})$ and A:

292
$$\delta(\text{NO}_2) - \delta(\text{NO}) = \frac{(\alpha_2 - \alpha_1) A + (\alpha(\text{NO}_2\text{-NO}) - 1)}{\alpha_2 A + \alpha(\text{NO}_2\text{-NO})} (1 + \delta(\text{NO}_2))$$

 293
$$\approx \frac{(\alpha_2 - \alpha_1) A + (\alpha(\text{NO}_2\text{-NO}) - 1)}{A + 1} (1 + \delta(\text{NO}_2))$$
 Eq. (7)

294
$$\delta(\text{NO}_2) - \delta(\text{NO}_x) = \frac{(\alpha_2 - \alpha_1) A + (\alpha(\text{NO}_2\text{-NO}) - 1)}{\alpha_2 A + \alpha(\text{NO}_2\text{-NO})} (1 + \delta(\text{NO}_2))(1 - f(\text{NO}_2))$$

 295
$$\approx \frac{(\alpha_2 - \alpha_1) A + (\alpha(\text{NO}_2\text{-NO}) - 1)}{A + 1} (1 + \delta(\text{NO}_2))(1 - f(\text{NO}_2))$$
 Eq. (8)

296 Equation (7) shows the isotopic fractionation between NO and NO₂ ($\delta(\text{NO}_2)$ - $\delta(\text{NO})$) is mainly
 297 determined by A, the EIE factor ($\alpha(\text{NO}_2\text{-NO})-1$) and the $(\alpha_2-\alpha_1)$ factor assuming $(1+\delta(\text{NO}_2))$ is
 298 close to 1. This $(\alpha_2-\alpha_1)$ represents a combination of KIE and PHIFE, suggesting they act together
 299 as one factor; therefore, we name the $(\alpha_2-\alpha_1)$ factor Leighton Cycle Isotopic Effect, i.e., LCIE.

300 Using measured $\delta(\text{NO}_2)$, $\delta(\text{NO}_x)$ values, A values (Table 1), and the previously determined $\alpha(\text{NO}_2\text{-}$
 301 NO) value. We plot $\frac{\delta(\text{NO}_2) - \delta(\text{NO}_x)}{(1 + \delta(\text{NO}_2))(1 - f(\text{NO}_2))}$ (equals to $\frac{\delta(\text{NO}_2) - \delta(\text{NO})}{(1 + \delta(\text{NO}_2))}$) against A value and use Equations
 302 (7) and (8) to estimate the $(\alpha_2-\alpha_1)$ value (Fig. 1C). The plot shows that the best fit for the LCIE
 303 factor is (-10 ± 5) ‰ (Rooted Mean Square Error, RMSE, was lowest when $\alpha_2-\alpha_1 = -10\%$). The
 304 uncertainties in the LCIE factor are relatively higher than that of the EIE factor, mainly because
 305 of the accumulated analytical uncertainties at low NO_x and O₃ concentrations, and low A values
 306 (0.10-0.28) due to the relatively low $j(\text{NO}_2)$ value ($1.4 \times 10^{-3} \text{ s}^{-1}$) under the chamber irradiation
 307 conditions.

308 This LCIE factor determined in our experiments is in good agreement with theoretical
 309 calculations. Walters and Michalski (2016) previously used an *ab initio* approach to determine an

Deleted: →

Deleted: $\frac{(\alpha_2 - \alpha_1) A + (\alpha(\text{NO}_2\text{-NO}) - 1)}{A + 1} (1 + \delta(\text{NO}))$ →

Formatted: Normal (Web), Left

Deleted: →

Deleted: $= \frac{(\alpha_2 - \alpha_1) A + (\alpha(\text{NO}_2\text{-NO}) - 1)}{A + 1} (1 + \delta(\text{NO}))(1 - f(\text{NO}_2))$

Deleted: NO

Deleted: $\delta(\text{NO}_2) - \delta(\text{NO})$

Deleted: $(1 + \delta(\text{NO}))$

Deleted: .

Moved (insertion) [2]

Deleted: EIE factor, we calculated

Deleted: was

Deleted: showing the lowest

Deleted: of 1.1%, Fig.

Moved up [2]: 1C).

324 α_2 value of 0.9933 at room temperature, 0.9943 at 237 K and 0.9929 at 310 K. The total variation
325 of α_2 values from 273 K to 310 K is only 1.4 ‰, significantly smaller than our experimental
326 uncertainty (± 5 ‰). The α_1 value was calculated using a ZPE shift model (Miller & Yung, 2000)
327 to calculate the isotopic fractionation of NO₂ by photolysis. Briefly, this model assumes both
328 isotopologues have the same quantum yield function and the PHIFE was only caused by the
329 differences in the ¹⁵NO₂ and ¹⁴NO₂ absorption cross-section as a function of wavelength, thus α_1
330 values do not vary by temperature. The ¹⁵NO₂ absorption cross-section was calculated by shifting
331 the ¹⁴NO₂ absorption cross-section by the ¹⁵NO₂ zero-point energy (Michalski et al., 2004). When
332 the ZPE shift model was used with the irradiation spectrum of the chamber lights, the resulting α_1
333 value was 1.0023. Therefore, the theoretically predicted α_2 - α_1 value should be -0.0090, i.e., (-
334 9.0 \pm 0.7) ‰ when temperature ranges from 273 K to 310 K. This result shows excellent agreement
335 with our experimentally determined room temperature α_2 - α_1 value of (-10 \pm 5) ‰.

336 This model was then used to evaluate the variations of α_1 value to different lighting
337 conditions. The TUV model (TUV5.3.2, Madronich & Flocke, 1999) was used to calculate the
338 solar wavelength spectrum at three different conditions: early morning/late afternoon (solar zenith
339 angle=85 degree), mid-morning/afternoon (solar zenith angle=45 degree), noon (solar zenith
340 angle=0 degree). These spectrums were used in the ZPE shift model to calculate the α_1 values,
341 which are 1.0025, 1.0028, and 1.0029 at solar zenith angles of 85, 45 and 0 degree, respectively.
342 These values, along with the predicted α_1 value in the chamber, showed a total span of 0.6‰
343 (1.0026 \pm 0.0003), which is again significantly smaller than our measured uncertainty. Therefore,
344 we suggest that our experimentally determined LCIE factor ((-10 \pm 5) ‰) can be used in most
345 tropospheric solar irradiation spectrums.

346 The equations can also be applied in tropospheric environments to calculate the combined
347 isotopic fractionations of EIE and LCIE for NO and NO₂. First, the NO₂ sink reactions (mainly
348 NO₂+OH in the daytime) are at least 2-3 orders of magnitude slower than the Leighton cycle and
349 the NO-NO₂ isotope exchange reactions (Walters et al., 2016), therefore their effects on the δ(NO₂)
350 should be minor. Second, although the conversion of NO into NO₂ in the ambient environment is
351 also controlled by NO + RO₂ and HO₂ in addition to NO+O₃ (e.g., King et al., 2001), Eq. (7) still
352 showed good agreement with field observations in previous studies. Freyer et al. (1993)
353 determined the annual average daytime δ(NO₂)-δ(NO) at Julich, Germany along with average
354 daytime NO concentration (9 nmol mol⁻¹, similar to our experimental conditions) to be
355 (+18.03±0.98) ‰. Using Eq. (7), assuming the daytime average *j*(NO₂) value throughout the year
356 was (5.0±1.0)×10⁻³, and a calculated A value from measured NO_x concentration ranged from 0.22-
357 0.33, the average NO-NO₂ fractionation factor was calculated to be (+19.8±1.4) ‰ (Fig. 1C), in
358 excellent agreement with the measurements in the present study. This agreement suggests the
359 NO+RO₂/HO₂ reactions might have similar fractionation factors as NO+O₃. Therefore, we suggest
360 Eq. (7) and (8) can be used to estimate the isotopic fractionations between NO and NO₂ in the
361 troposphere.

Deleted: 18

362

363 3.3 Calculating nitrogen isotopic fractionations of NO-NO₂

364 First, Eq. (7) was used to calculate the Δ(NO₂-NO) = δ(NO₂)-δ(NO) at a wide range of
365 NO_x concentrations, *f*(NO₂) and *j*(NO₂) values (Fig. 2A-D), assuming (1+δ(NO₂)) ≈ 1. *j*(NO₂)
366 values of 0 s⁻¹ (Fig. 2A), 1.4×10⁻³ s⁻¹ (Fig. 2B), 5×10⁻³ s⁻¹ (Fig. 2C) and 1×10⁻² s⁻¹ (Fig. 2D) were
367 selected to represent nighttime, dawn (as well as the laboratory conditions of our experiments),
368 daytime average and noon, respectively. Each panel represented a fixed *j*(NO₂) value, and the

Deleted: NO)=

371 $\Delta(\text{NO}_2\text{-NO})$ values were calculated as a function of the A value, which was derived from NO_x
372 concentration and $f(\text{NO}_2)$. The A values have a large span, from 0 to 500, depending on the $j(\text{NO}_2)$
373 value and the NO concentration. When $A=0$ ($j(\text{NO}_2)=0$) and $f(\text{NO}_2)<1$ (meaning NO- NO_2 coexist
374 and $[\text{O}_3]=0$), Eq. (7) and (8) become Eq. (2) and (3), showing the EIE was the sole factor, the
375 $\Delta(\text{NO}_2\text{-NO})$ values were solely controlled by EIE which has a constant value of +28.9 ‰ at 298K
376 (Fig. 2A). When $j(\text{NO}_2)>0$, the calculated $\Delta(\text{NO}_2\text{-NO})$ values showed a wide range from -10.0 ‰
377 (controlled by LCIE factor: $\alpha_2-\alpha_1=-10$ ‰) to +28.9 ‰ (controlled by EIE factor: $\alpha(\text{NO}_2\text{-NO})-1 =$
378 +28.9 ‰). Fig. 2B-D display the transition from a LCIE-dominated regime to an EIE-dominated
379 regime. The LCIE-dominated regime is characterized by low $[\text{NO}_x]$ (<50 pmol mol⁻¹), representing
380 remote ocean areas and polar regions (Beine et al., 2002; Custard et al., 2015). At this range the A
381 value can be greater than 200, thus Eq. (7) can be simplified as: $\Delta(\text{NO}_2\text{-NO}) = \alpha_2-\alpha_1$, suggesting
382 the LCIE almost exclusively controls the NO- NO_2 isotopic fractionation. The $\Delta(\text{NO}_2\text{-NO})$ values
383 of these regions are predicted to be <0 ‰ during most time of the day and <-5 ‰ at noon. On the
384 other hand, the EIE-dominated regime was characterized by high $[\text{NO}_x]$ (>20 nmol mol⁻¹) and low
385 $f(\text{NO}_2)$ (<0.6), representative of regions with intensive NO emissions, e.g., near roadside or stack
386 plumes (Clapp & Jenkin, 2001; Kimbrough et al., 2017). In this case, the τ_{exchange} are relatively
387 short (10-50 s) compared to the τ_{photo} (approximately 100 s at noon and 1000 s at dawn), therefore
388 the A values are small (0.01-0.5). The EIE factor in this regime thus is much more important than
389 the LCIE factor, resulting in high $\Delta(\text{NO}_2\text{-NO})$ values (>20 ‰). Between the two regimes, both
390 EIE and LCIE are competitive and therefore it is necessary to use Eq. (7) to quantify the $\Delta(\text{NO}_2\text{-}$
391 NO) values.

392 Fig. 2 also implies that changes in the $j(\text{NO}_2)$ value can cause the diurnal variations in
393 $\Delta(\text{NO}_2\text{-NO})$ values. Changing $j(\text{NO}_2)$ would affect the value of A and consequently the NO- NO_2

Deleted: 27.5

Deleted: 27.5

Deleted: 27.5

397 isotopic fractionations in two ways: 1) changes in $j(\text{NO}_2)$ value would change the photolysis
398 intensity, therefore the τ_{photo} value; 2) in addition, changes in $j(\text{NO}_2)$ value would also alter the
399 steady state NO concentration, therefore changing the τ_{exchange} (Fig. 2C). The combined effect of
400 these two factors on the A value varies along with the atmospheric conditions, and thus needs to
401 be carefully calculated using NO_x concentration data and atmospheric chemistry models.

402 We then calculated the differences of $\delta^{15}\text{N}$ values between NO_2 and total NO_x , e.g. $\Delta(\text{NO}_2-$
403 $\text{NO}_x) = \delta(\text{NO}_2) - \delta(\text{NO}_x)$ in Fig. 2E-H. Since $\Delta(\text{NO}_2-\text{NO}_x)$ are connected through the observed $\delta^{15}\text{N}$
404 of NO_2 (or nitrate) to the $\delta^{15}\text{N}$ of NO_x sources, this term might be useful in field studies (e.g.,
405 Chang et al., 2018; Zong et al., 2017). The calculated $\Delta(\text{NO}_2-\text{NO}_x)$ values (Fig. 2E-H) also showed
406 a LCIE-dominated regime at low $[\text{NO}_x]$ and an EIE-dominated regime at high $[\text{NO}_x]$. The $\Delta(\text{NO}_2-$
407 $\text{NO}_x)$ values were dampened by the $1-f(\text{NO}_2)$ factor comparing to $\Delta(\text{NO}_2-\text{NO})$, as shown in Eq.
408 (3) and (8): $\Delta(\text{NO}_2-\text{NO}_x) = \Delta(\text{NO}_2-\text{NO})(1-f(\text{NO}_2))$. At high $f(\text{NO}_2)$ values (>0.8), the differences
409 between $\delta(\text{NO}_2)$ and $\delta(\text{NO}_x)$ were less than 5 ‰, thus the measured $\delta(\text{NO}_2)$ values were similar to
410 $\delta(\text{NO}_x)$, although the isotopic fractionation between NO and NO_2 could be noteworthy. Some
411 ambient environments with significant NO emissions or high NO_2 photolysis rates usually have
412 $f(\text{NO}_2)$ values between 0.4-0.8 (Mazzeo et al., 2005; Vicars et al., 2013). In this scenario, the
413 $\Delta(\text{NO}_2-\text{NO}_x)$ values in Fig. 2F-H showed wide ranges of -4.8 ‰ to +15.6 ‰, -6.0 ‰ to +15.0 ‰,
414 and -6.3 ‰ to +14.2 ‰ at $j(\text{NO}_2)=1.4 \times 10^{-3} \text{ s}^{-1}$, $5 \times 10^{-3} \text{ s}^{-1}$, $1 \times 10^{-2} \text{ s}^{-1}$, respectively. These significant
415 differences again highlighted the importance of both LCIE and EIE (Eq. (7) and (8)) in calculating
416 the $\Delta(\text{NO}_2-\text{NO}_x)$. In the following discussion, we assume 1) the α_1 value remain constant (see
417 discussion above), 2) the $\text{NO}+\text{RO}_2/\text{HO}_2$ reactions have the same fractionation factors (α_2) as
418 $\text{NO}+\text{O}_3$, and 3) both EIE and LCIE do not display significant temperature dependence, then use

419 Equations (7) and (8) and this laboratory determined LCIE factor (-10 ‰) to calculate the nitrogen
420 isotopic fractionation between NO and NO₂ at various tropospheric atmospheric conditions.

421

422 4. Implications

423 The daily variations of $\Delta(\text{NO}_2\text{-NO}_x)$ values at two roadside NO_x monitoring sites were
424 predicted to demonstrate the effects of NO_x concentrations to the NO-NO₂ isotopic fractionations.

425 Hourly NO and NO₂ concentrations were acquired from a roadside site at Anaheim, CA
426 (<https://www.arb.ca.gov>) and an urban site at Evansville, IN (<http://idem.tx.sutron.com>) on July

427 25, 2018. The hourly $f(\text{NO}_2)$ values output from the TUV model (Madronich & Flocke, 1999) at
428 these locations was used to calculate the daily variations of $\Delta(\text{NO}_2\text{-NO}_x)$ values (Fig. 3A, B) by

429 applying Eq. (8) and assuming $(1+\delta(\text{NO}_2)) \approx 1$. Hourly NO_x concentrations were 12-51 nmol mol⁻¹
430 at Anaheim and 9-38 nmol mol⁻¹ at Evansville and the $f(\text{NO}_2)$ values at both sites did not show

431 significant daily variations (0.45±0.07 at Anaheim and 0.65±0.08 at Evansville), likely because
432 the NO_x concentrations were controlled by the high NO emissions from the road (Gao, 2007). The

433 calculated $\Delta(\text{NO}_2\text{-NO}_x)$ values using Eq. (8) showed significant diurnal variations. During the
434 nighttime, the isotopic fractionations were solely controlled by the EIE, the predicted $\Delta(\text{NO}_2\text{-NO}_x)$

435 values were (+14.5±2.0) ‰ and (+8.7±2.1) ‰ at Anaheim and Evansville, respectively. During
436 the daytime, the existence of LCIE lowered the predicted $\Delta(\text{NO}_2\text{-NO}_x)$ values to (+9.8±1.7) ‰ at

437 Anaheim and (+3.1±1.5) ‰ at Evansville while the $f(\text{NO}_2)$ values at both sites remained similar.
438 The lowest $\Delta(\text{NO}_2\text{-NO}_x)$ values for both sites (+7.0 ‰ and +1.7 ‰) occurred around noon when

439 the NO_x photolysis was the most intense. In contrast, if one neglects the LCIE factor in the daytime,
440 the $\Delta(\text{NO}_2\text{-NO}_x)$ values would be (+12.9±1.5) ‰ and (+10.0±1.6) ‰ respectively, an

441 overestimation of 3.1 ‰ and 6.9 ‰. These discrepancies suggested that the LCIE played an

Deleted: NO)=

443 important role in the NO-NO₂ isotopic fractionations and neglecting it could bias the NO_x source
444 apportionment using δ¹⁵N of NO₂ or nitrate.

445 The role of LCIE was more important in less polluted sites. The Δ(NO₂-NO_x) values
446 calculated for a suburban site near San Diego, CA, USA, again using the hourly NO_x
447 concentrations (<https://www.arb.ca.gov>, Fig. 3C) and *f*(NO₂) values calculated from the TUV
448 model. NO_x concentrations at this site varied from 1 to 9 nmol mol⁻¹ and assuming (1+δ(NO₂)) ≈ 1.
449 During the nighttime, NO_x was in the form of NO₂ (*f*(NO₂) = 1) because O₃ concentrations were
450 higher than NO_x, thus the δ(NO₂) values should be identical to δ(NO_x) (Δ(NO₂-NO_x) = 0). In the
451 daytime a certain amount of NO was produced by direct NO emission and NO₂ photolysis but the
452 *f*(NO₂) was still high (0.73±0.08). Our calculation suggested the daytime Δ(NO₂-NO_x) values
453 should be only (+1.3±3.2) ‰ with a lowest value of -1.3 ‰. These Δ(NO₂-NO_x) values were
454 similar to the observed and modeled summer daytime δ(NO₂) values in West Lafayette, IN
455 (Walters et al., 2018), which suggest the average daytime Δ(NO₂-NO_x) values at NO_x = (3.9±1.2)
456 nmol mol⁻¹ should range from +0.1 ‰ to +2.4 ‰. In this regime, we suggest the Δ(NO₂-NO_x)
457 values were generally small due to the significant contribution of LCIE and high *f*(NO₂).

458 The LCIE should be the dominant factor controlling the NO-NO₂ isotopic fractionation at
459 remote regions, resulting in a completely different diurnal pattern of Δ(NO₂-NO_x) compared with
460 the urban-suburban area. Direct hourly measurements of NO_x at remote sites are rare, thus we used
461 total NO_x concentration of 50 pmol mol⁻¹, daily O₃ concentration of 20 nmol mol⁻¹ at Summit,
462 Greenland (Dibb et al., 2002; Hastings et al., 2004; Honrath et al., 1999; Yang et al., 2002), and
463 assumed (1+δ(NO₂)) ≈ 1 and the conversion of NO to NO₂ was completely controlled by O₃ to
464 calculate the NO/NO₂ ratios. Here the isotopes of NO_x were almost exclusively controlled by the
465 LCIE due to the high A values (>110). The Δ(NO₂-NO_x) values displayed a clear diurnal pattern

Deleted: NO)=

Deleted: NO)=

468 (Fig. 3D) with highest value of -0.3 ‰ in the “nighttime” (solar zenith angle >85 degree) and
469 lowest value of -5.0 ‰ in the mid-day. This suggest that the isotopic fractionations between NO
470 and NO₂ were almost completely controlled by LCIE at remote regions, when NO_x concentrations
471 were <0.1 nmol mol⁻¹. However, since the isotopic fractionation factors of nitrate-formation
472 reactions (NO₂+OH, NO₃+HC, N₂O₅+H₂O) are still unknown, more studies are needed to fully
473 explain the daily and seasonal variations of δ(NO₃⁻) at remote regions.

474 Nevertheless, our results have a few limitations. First, currently there are very few field
475 observations that can be used to evaluate our model, therefore, future field observations that
476 measure the δ¹⁵N values of ambient NO and NO₂ should be carried out to test our model. Second,
477 more work, including theoretical and experimental studies, is needed to investigate the isotope
478 fractionation factors occurring during the conversion from NO_x to NO_y and nitrate: in the NO_y
479 cycle, EIE (isotopic exchange between NO₂, NO₃ and N₂O₅), KIE (formation of NO₃, N₂O₅ and
480 nitrate) and PHIFE (photolysis of NO₃, N₂O₅, HONO and sometimes nitrate) may also exist and
481 be relevant for the δ¹⁵N of HNO₃ and HONO. In particular, the N isotope fractionation occurring
482 during the NO₂ + OH → HNO₃ reaction needs investigation. Such studies could help us modeling
483 the isotopic fractionation between NO_x emission and nitrate, and eventually enable us to analyze
484 the δ¹⁵N value of NO_x emission by measuring the δ¹⁵N values of nitrate aerosols and nitrate in wet
485 depositions. Third, our discussion only focuses on the reactive nitrogen chemistry in the
486 troposphere, however, the nitrogen chemistry in the stratosphere is drastically different from the
487 tropospheric chemistry, thus future studies are also needed to investigate the isotopic fractionations
488 in the stratospheric nitrogen chemistry. Last, the temperature dependence of both EIE and LCIE
489 needs to be carefully investigated, because of the wide range of temperature in both troposphere
490 and stratosphere. Changes in temperature could alter the isotopic fractionation factors of both EIE

491 and LCIE, as well as contribute to the seasonality of isotopic fractionations between NO_x and NO_y
492 molecules.

493

494 5. Conclusions

495 The effect of NO_x photochemistry on the nitrogen isotopic fractionations between NO and
496 NO₂ was investigated. We first measured the isotopic fractionations between NO and NO₂ and
497 provided mathematical solutions to assess the impact of NO_x level and NO₂ photolysis rate ($j(\text{NO}_2)$)
498 to the relative importance of EIE and LCIE. The EIE and LCIE isotope fractionation factors, at
499 room temperature, were determined to be 1.0289 ± 0.0019 and 0.990 ± 0.005 , respectively. These
500 calculations and measurements can be used to determine the steady state $\Delta(\text{NO}_2\text{-NO})$ and $\Delta(\text{NO}_2\text{-}$
501 $\text{NO}_x)$ values at room temperature. Subsequently we applied our equations to polluted, clean and
502 remote sites to model the daily variations of $\Delta(\text{NO}_2\text{-NO}_x)$ values. We found that the $\Delta(\text{NO}_2\text{-NO}_x)$
503 values could vary from over +20 ‰ to less than -5 ‰ depending on the environment: in general,
504 the role of LCIE becoming more important at low NO_x concentrations, which tend to decrease the
505 $\Delta(\text{NO}_2\text{-NO}_x)$ values. Our work provided a mathematical approach to quantify the nitrogen isotopic
506 fractionations between NO and NO₂ that can be applied to many tropospheric environments, which
507 could help interpret the measured $\delta^{15}\text{N}$ values of NO₂ and nitrate in field observation studies.

508

509 Acknowledgement

510 We thank NCAR's Advanced Study Program granted to Jianghanyang Li. The National
511 Center for Atmospheric Research is operated by the University Corporation for Atmospheric
512 Research, under the sponsorship of the National Science Foundation. We also thank funding

Deleted: 0275

Deleted: 0012

515 support from Purdue Climate Change Research Center and A. H. Ismail Interdisciplinary Program
516 Doctoral Research Travel Award granted by Purdue University.

517 **Data Availability**

518 Data acquired from this study was deposited at Open Sciences Framework (Li, 2019,
519 DOI 10.17605/OSF.IO/JW8HU).

520 **Author contribution**

521 J. Li and G. Michalski designed the experiments, X. Zhang and J. Li conducted the
522 experiments. X. Zhang, G. Michalski, J. Orlando and G. Tyndall helped J. Li in interpreting the
523 results. The manuscript was written by J. Li and all the authors have contributed during the revision
524 of this manuscript.

525 **Competing interest**

526 The authors declare no competing interest.

527

528 **References:**

529
530 Atkinson, R., Baulch, D. L., Cox, R. A., Crowley, J. N., Hampson, R. F., Hynes, R. G., Jenkin, M.
531 E., Rossi, M. J., and Troe, J. (2004). Evaluated kinetic and photochemical data for atmospheric
532 chemistry: Volume I-gas phase reactions of O_x, HO_x, NO_x and SO_x. *Atmospheric chemistry and*
533 *physics*, 4(6), 1461-1738. <https://doi.org/10.5194/acp-4-1461-2004>, 2004.

534
535 Barney, W. S., & Finlayson-Pitts, B. J. (2000). Enhancement of N₂O₄ on porous glass at room
536 temperature: A key intermediate in the heterogeneous hydrolysis of NO₂? *The Journal of Physical*
537 *Chemistry A*, 104(2), 171–175. <https://doi.org/10.1021/jp993169b>

538
539 Begun, G. M., & Fletcher, W. H. (1960). Partition function ratios for molecules containing
540 nitrogen isotopes. *The Journal of Chemical Physics*, 33(4), 1083–1085.
541 <https://doi.org/10.1063/1.1731338>

542
543 Begun, G. M., & Melton, C. E. (1956). Nitrogen isotopic fractionation between NO and NO₂ and
544 mass discrimination in mass analysis of NO₂. *The Journal of Chemical Physics*, 25(6), 1292–1293.
545 <https://doi.org/10.1063/1.1743215>

546

547 Beine, H. J., Honrath, R. E., Dominé, F., Simpson, W. R., & Fuentes, J. D. (2002). NO_x during
548 background and ozone depletion periods at Alert: Fluxes above the snow surface. *Journal of*
549 *Geophysical Research: Atmospheres*, 107(D21), ACH-7. <https://doi.org/10.1029/2002JD002082>
550

551 Bigeleisen, J., & Mayer, M. G. (1947). Calculation of equilibrium constants for isotopic exchange
552 reactions. *The Journal of Chemical Physics*, 15(5), 261-267. <https://doi.org/10.1063/1.1746492>
553

554 Bigeleisen, J., & Wolfsberg, M. (1957). Theoretical and experimental aspects of isotope effects in
555 chemical kinetics. *Advances in Chemical Physics*, 15-76.
556 <https://doi.org/10.1002/9780470143476.ch2>
557

558 Casciotti, K. L., & McIlvin, M. R. (2007). Isotopic analyses of nitrate and nitrite from reference
559 mixtures and application to Eastern Tropical North Pacific waters. *Marine Chemistry*, 107(2), 184-
560 201. <https://doi.org/10.1016/j.marchem.2007.06.021>
561

562 Chang, Y., Zhang, Y., Tian, C., Zhang, S., Ma, X., Cao, F., et al. (2018). Nitrogen isotope
563 fractionation during gas-to-particle conversion of NO_x to NO₃⁻ in the atmosphere—implications for
564 isotope-based NO_x source apportionment. *Atmospheric Chemistry and Physics*, 18(16), 11647-
565 11661. <https://doi.org/10.5194/acp-18-11647-2018>, 2018.
566

567 Clapp, L. J., & Jenkin, M. E. (2001). Analysis of the relationship between ambient levels of O₃,
568 NO₂ and NO as a function of NO_x in the UK. *Atmospheric Environment*, 35(36), 6391-6405.
569 [https://doi.org/10.1016/S1352-2310\(01\)00378-8](https://doi.org/10.1016/S1352-2310(01)00378-8)
570

571 Custard, K. D., Thompson, C. R., Pratt, K. A., Shepson, P. B., Liao, J., Huey, L. G., Orlando, J. J.,
572 Weinheimer, A. J., Apel, E., Hall, S. R., Flocke, F., Mauldin, L., Hornbrook, R. S., Pöhler, D.,
573 General, S., Zielcke, J., Simpson, W. R., Platt, U., Fried, A., Weibring, P., Sive, B. C., Ullmann,
574 K., Cantrell, C., Knapp, D. J., and Montzka, D. D.: The NO_x dependence of bromine chemistry in
575 the Arctic atmospheric boundary layer, *Atmos. Chem. Phys.*, 15, 10799-10809,
576 <https://doi.org/10.5194/acp-15-10799-2015>, 2015.
577

578 Dibb, J. E., Arsenaault, M., Peterson, M. C., & Honrath, R. E. (2002). Fast nitrogen oxide
579 photochemistry in Summit, Greenland snow. *Atmospheric Environment*, 36(15-16), 2501-2511.
580 [https://doi.org/10.1016/S1352-2310\(02\)00130-9](https://doi.org/10.1016/S1352-2310(02)00130-9)
581

582 Do Remus, R. H., Mehrotra, Y., Lanford, W. A., & Burman, C. (1983). Reaction of water with
583 glass: influence of a transformed surface layer. *Journal of Materials Science*, 18(2), 612-622.
584 <https://doi.org/10.1007/BF00560651>
585

586 Elliott, E. M., Kendall, C., Boyer, E. W., Burns, D. A., Lear, G. G., Golden, H. E., Harlin, K.,
587 Bytnerowicz, A., Butler, T. J., and Glatz, R. (2009). Dual nitrate isotopes in dry deposition: Utility
588 for partitioning NO_x source contributions to landscape nitrogen deposition. *Journal of Geophysical*
589 *Research: Biogeosciences*, 114(G4), G04020. <https://doi.org/10.1029/2008JG000889>
590

591 Felix, J. D., & Elliott, E. M. (2014). Isotopic composition of passively collected nitrogen dioxide
592 emissions: Vehicle, soil and livestock source signatures. *Atmospheric Environment*, 92, 359–366.
593 <https://doi.org/10.1016/j.atmosenv.2014.04.005>
594

595 Felix, J. D., Elliott, E. M., & Shaw, S. L. (2012). Nitrogen isotopic composition of coal-fired power
596 plant NO_x: influence of emission controls and implications for global emission inventories.
597 *Environmental Science & Technology*, 46(6), 3528–3535. <https://doi.org/10.1021/es203355v>
598

599 Frey, M. M., Savarino, J., Morin, S., Erbland, J., & Martins, J. M. F. (2009). Photolysis imprint in
600 the nitrate stable isotope signal in snow and atmosphere of East Antarctica and implications for
601 reactive nitrogen cycling. *Atmos. Chem. Phys.*, 9, 8681–8696. [https://doi.org/10.5194/acp-9-8681-](https://doi.org/10.5194/acp-9-8681-2009)
602 2009, 2009.
603

604 Freyer, H. D. (1991). Seasonal variation of ¹⁵N/¹⁴N ratios in atmospheric nitrate species. *Tellus B*,
605 43(1), 30–44. <https://doi.org/10.1034/j.1600-0889.1991.00003.x>
606

607 Freyer, H. D., Kley, D., Volz-Thomas, A., & Kobel, K. (1993). On the interaction of isotopic
608 exchange processes with photochemical reactions in atmospheric oxides of nitrogen. *Journal of*
609 *Geophysical Research: Atmospheres*, 98(D8), 14791–14796. <https://doi.org/10.1029/93JD00874>
610

611 Gao, H. O. (2007). Day of week effects on diurnal ozone/NO_x cycles and transportation emissions
612 in Southern California. *Transportation Research Part D: Transport and Environment*, 12(4), 292–
613 305. <https://doi.org/10.1016/j.trd.2007.03.004>
614

615 Gobel, A. R., Altieri, K. E., Peters, A. J., Hastings, M. G., & Sigman, D. M. (2013). Insights into
616 anthropogenic nitrogen deposition to the North Atlantic investigated using the isotopic
617 composition of aerosol and rainwater nitrate. *Geophysical Research Letters*, 40(22), 5977–5982.
618 <https://doi.org/10.1002/2013GL058167>
619

620 Hastings, M G, Jarvis, J. C., & Steig, E. J. (2009). Anthropogenic impacts on nitrogen isotopes of
621 ice-core nitrate. *Science*, 324(5932), 1288. DOI: 10.1126/science.1170510
622

623 Hastings, M G, Steig, E. J., & Sigman, D. M. (2004). Seasonal variations in N and O isotopes of
624 nitrate in snow at Summit, Greenland: Implications for the study of nitrate in snow and ice cores.
625 *Journal of Geophysical Research: Atmospheres*, 109(D20).
626 <https://doi.org/10.1029/2004JD004991>
627

628 Honrath, R. E., Peterson, M. C., Guo, S., Dibb, J. E., Shepson, P. B., & Campbell, B. (1999).
629 Evidence of NO_x production within or upon ice particles in the Greenland snowpack. *Geophysical*
630 *Research Letters*, 26(6), 695–698. <https://doi.org/10.1029/1999GL900077>
631

632 Jarvis, J. C., Steig, E. J., Hastings, M. G., & Kunasek, S. A. (2008). Influence of local
633 photochemistry on isotopes of nitrate in Greenland snow. *Geophysical Research Letters*, 35(21).
634 <https://doi.org/10.1029/2008GL035551>
635

636 Kendall, C., Elliott, E. M., & Wankel, S. D. (2007). Tracing anthropogenic inputs of nitrogen to
637 ecosystems. *Stable Isotopes in Ecology and Environmental Science*, 2, 375–449.
638 <https://doi.org/10.1002/9780470691854.ch12>
639

640 Kimbrough, S., Owen, R. C., Snyder, M., & Richmond-Bryant, J. (2017). NO to NO₂ conversion
641 rate analysis and implications for dispersion model chemistry methods using Las Vegas, Nevada
642 near-road field measurements. *Atmospheric Environment*, 165, 23–34.
643 <https://doi.org/10.1016/j.atmosenv.2017.06.027>
644

645 King, M. D., Canosa-Mas, C. E. and Wayne R. P. (2001). Gas-phase reactions between RO₂ and
646 NO, HO₂ or CH₃O₂: correlations between rate constants and the SOMO energy of the peroxy (RO₂)
647 radical. *Atmospheric Environment* 35.12 (2001): 2081-2088. [https://doi.org/10.1016/S1352-](https://doi.org/10.1016/S1352-2310(00)00501-X)
648 [2310\(00\)00501-X](https://doi.org/10.1016/S1352-2310(00)00501-X)
649

650 Knote, C., Tuccella, P., Curci, G., Emmons, L., Orlando, J. J. Madronich, S., Baró, R., Jiménez-
651 Guerrero, P., Luecken, D., Hogrefe, C., Forkel, R., Werhahn, J., Hirtl, M., Pérez, J. L., San José,
652 R., Giordano, L., Brunner, D., Yahya, K., Zhang, Y., Influence of the choice of gas-phase
653 mechanism on predictions of key gaseous pollutants during the AQMEII phase-2 intercomparison.
654 *Atmospheric Environment* 115 (2015): 553-568. <https://doi.org/10.1016/j.atmosenv.2014.11.066>.
655

656 Li, J. (2019). Quantifying the nitrogen equilibrium and photochemistry-induced kinetic isotopic
657 effects between NO and NO₂. Retrieved from osf.io/jw8hu
658

659 Madronich, S., & Flocke, S. (1999). The role of solar radiation in atmospheric chemistry. In
660 *Environmental photochemistry* (pp. 1–26). *The Handbook of Environmental Chemistry (Reactions*
661 *and Processes)*, vol 2 / 2L. Springer, Berlin, Heidelberg. [https://doi.org/10.1007/978-3-540-69044-](https://doi.org/10.1007/978-3-540-69044-3_1)
662 [3_1](https://doi.org/10.1007/978-3-540-69044-3_1)
663

664 Mazzeo, N. A., Venegas, L. E., & Choren, H. (2005). Analysis of NO, NO₂, O₃ and NO_x
665 concentrations measured at a green area of Buenos Aires City during wintertime. *Atmospheric*
666 *Environment*, 39(17), 3055–3068. <https://doi.org/10.1016/j.atmosenv.2005.01.029>
667

668 McIlvin, M. R., & Altabet, M. A. (2005). Chemical conversion of nitrate and nitrite to nitrous
669 oxide for nitrogen and oxygen isotopic analysis in freshwater and seawater. *Analytical Chemistry*,
670 77(17), 5589–5595. <https://doi.org/10.1021/ac050528s>
671

672 Michalski, G., Jost, R., Sugny, D., Joyeux, M., & Thiemens, M. (2004). Dissociation energies of
673 six NO₂ isotopologues by laser induced fluorescence spectroscopy and zero-point energy of some
674 triatomic molecules. *The Journal of Chemical Physics*, 121(15), 7153–7161.
675 <https://doi.org/10.1063/1.1792233>
676

677 Michalski, G., Bockheim, J. G., Kendall, C., & Thiemens, M. (2005). Isotopic composition of
678 Antarctic Dry Valley nitrate: Implications for NO_x sources and cycling in Antarctica. *Geophysical*
679 *Research Letters*, 32(13). <https://doi.org/10.1029/2004GL022121>
680

681 Miller, C. E., & Yung, Y. L. (2000). Photo-induced isotopic fractionation. *Journal of Geophysical*
682 *Research: Atmospheres*, 105(D23), 29039–29051. <https://doi.org/10.1029/2000JD900388>
683

684 Monse, E. U., Spindel, W., & Stern, M. J. (1969). Analysis of isotope-effect calculations illustrated
685 with exchange equilibria among oxynitrogen compounds. Rutgers-The State Univ., Newark, NJ.
686 DOI: 10.1021/ba-1969-0089.ch009
687

688 Morin, S., Savarino, J., Frey, M. M., Domine, F., Jacobi, H.-W., Kaleschke, L., & Martins, J. M.
689 F. (2009). Comprehensive isotopic composition of atmospheric nitrate in the Atlantic Ocean
690 boundary layer from 65°S to 79°N. *J. Geophys. Res.*, 114. <https://doi.org/10.1029/2008JD010696>
691

692 Park, Y.-M., Park, K.-S., Kim, H., Yu, S.-M., Noh, S., Kim, M.-S., Kim, J.-Y., Ahn, J.-Y., Lee,
693 M.-D., Seok, K.-S., Kin, Y.-H., (2018). Characterizing isotopic compositions of TC-C, NO₃-N,
694 and NH₄⁺-N in PM_{2.5} in South Korea: Impact of China's winter heating.
695 <https://doi.org/10.1016/j.envpol.2017.10.072>
696

697 Saliba, N. A., Yang, H., & Finlayson-Pitts, B. J. (2001). Reaction of gaseous nitric oxide with
698 nitric acid on silica surfaces in the presence of water at room temperature. *The Journal of Physical*
699 *Chemistry A*, 105(45), 10339–10346. <https://doi.org/10.1021/jp012330r>
700

701 Savarino, J., Morin, S., Erbland, J., Grannec, F., Patey, M. D., Vicars, W., Alexander, B.,
702 Achterberg, E. P., (2013). Isotopic composition of atmospheric nitrate in a tropical marine
703 boundary layer. *Proceedings of the National Academy of Sciences*, 110(44), 17668–17673.
704 <https://doi.org/10.1073/pnas.1216639110>
705

706 Sharma, H. D., Jervis, R. E., & Wong, K. Y. (1970). Isotopic exchange reactions in nitrogen oxides.
707 *The Journal of Physical Chemistry*, 74(4), 923–933. <https://doi.org/10.1021/j100699a044>
708

709 Takei, T., Yamazaki, A., Watanabe, T., & Chikazawa, M. (1997). Water adsorption properties on
710 porous silica glass surface modified by trimethylsilyl groups. *Journal of Colloid and Interface*
711 *Science*, 188(2), 409–414. <https://doi.org/10.1006/jcis.1997.4777>
712

713 Urey, H. C. (1947). The thermodynamic properties of isotopic substances. *Journal of the Chemical*
714 *Society (Resumed)*, 562-581. <https://doi.org/10.1039/JR9470000562>
715

716 Vicars, W. C., Morin, S., Savarino, J., Wagner, N. L., Erbland, J., Vince, E., Martins, J. M. F.,
717 Lerner, B. M., Quinn, P. K., Coffman, D. J., Williams, E. J., Brown, S. S., (2013). Spatial and
718 diurnal variability in reactive nitrogen oxide chemistry as reflected in the isotopic composition of
719 atmospheric nitrate: Results from the CalNex 2010 field study. *Journal of Geophysical Research:*
720 *Atmospheres*, 118(18), 10–567. <https://doi.org/10.1002/jgrd.50680>
721

722 Walters, W. W., & Michalski, G. (2015). Theoretical calculation of nitrogen isotope equilibrium
723 exchange fractionation factors for various NO_y molecules. *Geochimica et Cosmochimica Acta*,
724 164, 284–297. <https://doi.org/10.1016/j.gca.2015.05.029>
725

726 Walters, W. W., Goodwin, S. R., & Michalski, G. (2015). Nitrogen stable isotope composition
727 ($\delta^{15}\text{N}$) of vehicle-emitted NO_x . *Environmental Science & Technology*, 49(4), 2278–2285.
728 <https://doi.org/10.1021/es505580v>
729

730 Walters, W. W., & Michalski, G. (2016). Ab initio study of nitrogen and position-specific oxygen
731 kinetic isotope effects in the $\text{NO}+\text{O}_3$ reaction. *The Journal of chemical physics*, 145(22), 224311.
732 <https://doi.org/10.1063/1.4968562>
733

734 Walters, W. W., Simonini, D. S., & Michalski, G. (2016). Nitrogen isotope exchange between NO
735 and NO_2 and its implications for $\delta^{15}\text{N}$ variations in tropospheric NO_x and atmospheric nitrate.
736 *Geophysical Research Letters*, 43(1), 440–448. <https://doi.org/10.1002/2015GL066438>
737

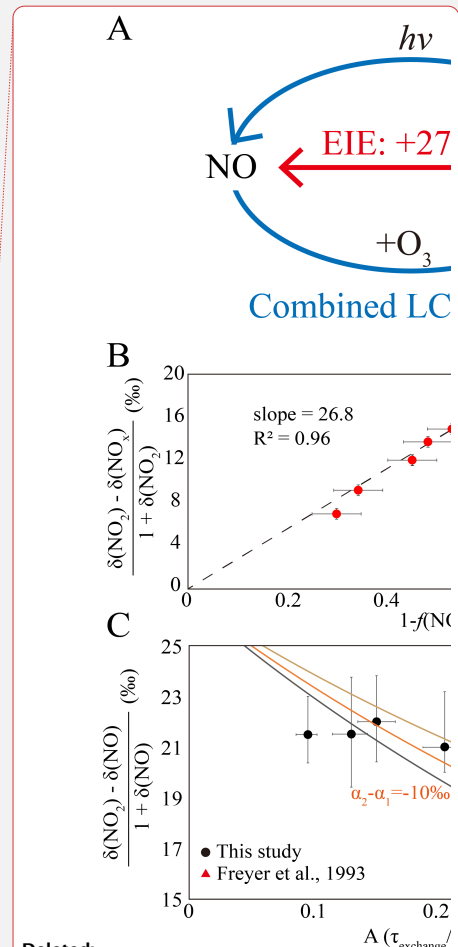
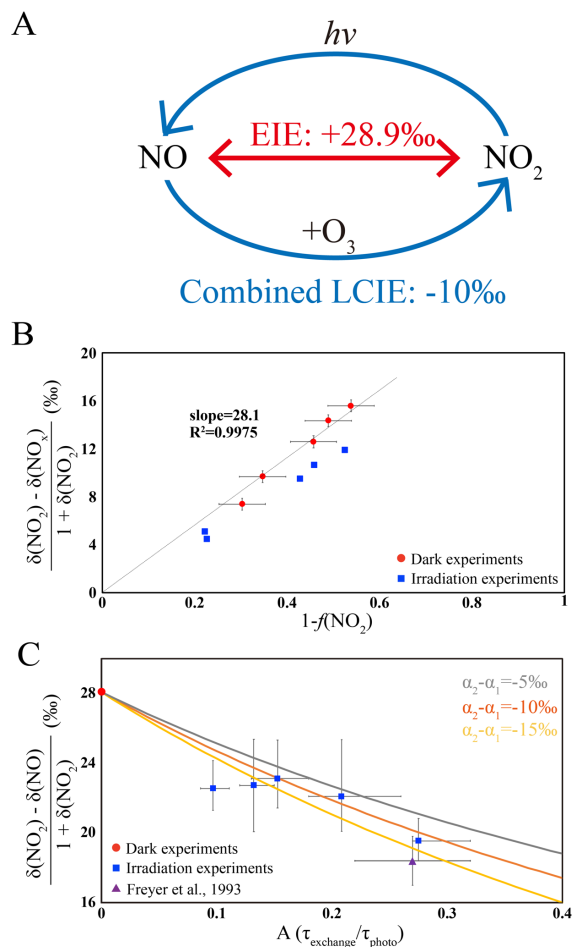
738 Walters, W. W., Fang, H., & Michalski, G. (2018). Summertime diurnal variations in the isotopic
739 composition of atmospheric nitrogen dioxide at a small midwestern United States city.
740 *Atmospheric Environment*, 179, 1–11. <https://doi.org/10.1016/j.atmosenv.2018.01.047>
741

742 Williams, E. L., & Grosjean, D. (1990). Removal of atmospheric oxidants with annular denuders.
743 *Environmental Science & Technology*, 24(6), 811–814. <https://doi.org/10.1021/es00076a002>
744

745 Yang, J., Honrath, R. E., Peterson, M. C., Dibb, J. E., Sumner, A. L., Shepson, P. B., Frey, M.,
746 Jacobi, H.-W., Swanson, A., Blake, N., (2002). Impacts of snowpack emissions on deduced levels
747 of OH and peroxy radicals at Summit, Greenland. *Atmospheric Environment*, 36(15–16), 2523–
748 2534. [https://doi.org/10.1016/S1352-2310\(02\)00128-0](https://doi.org/10.1016/S1352-2310(02)00128-0)
749

750 Zhang, X., Ortega, J., Huang, Y., Shertz, S., Tyndall, G. S., & Orlando, J. J. (2018). A steady-state
751 continuous flow chamber for the study of daytime and nighttime chemistry under atmospherically
752 relevant NO levels. *Atmospheric Measurement Techniques*, 11(5), 2537–2551.
753 <https://doi.org/10.5194/amt-11-2537-2018>
754

755 Zong, Z., Wang, X., Tian, C., Chen, Y., Fang, Y., Zhang, F., Li, C., Sun, J., Li, J., Zhang, G.,
756 (2017). First assessment of NO_x sources at a regional background site in North China using
757 isotopic analysis linked with modeling. *Environmental Science & Technology*, 51(11), 5923–5931.
758 <https://doi.org/10.1021/acs.est.6b06316>



759
760
761
762
763
764
765
766
767
768
769

Fig. 1 **A.** a sketch of the isotopic fractionation processes between NO and NO₂, both fractionation factors are determined in this work. **B.** Results from five dark experiments (red circles) yielded a line with slope of 28.1‰ and an $\alpha(\text{NO}_2\text{-NO})$ value of 1.0289, while the results from five UV irradiation experiments (blue squares) showed a smaller slope; **C.** Results from five UV irradiation experiments (blue squares) and a previous field study (purple triangle), comparing to the dark experiments (red circle). The three lines represent different $(\alpha_2 - \alpha_1)$ values: the $(\alpha_2 - \alpha_1) = -10\%$ line showed the lowest RMSE to our experimental data as well as the previous field observations. The error bars in panels B and C represented the combined uncertainties of NO_x concentration measurements and isotopic analysis.

Deleted:

Deleted: 0.0268

Deleted: 0275

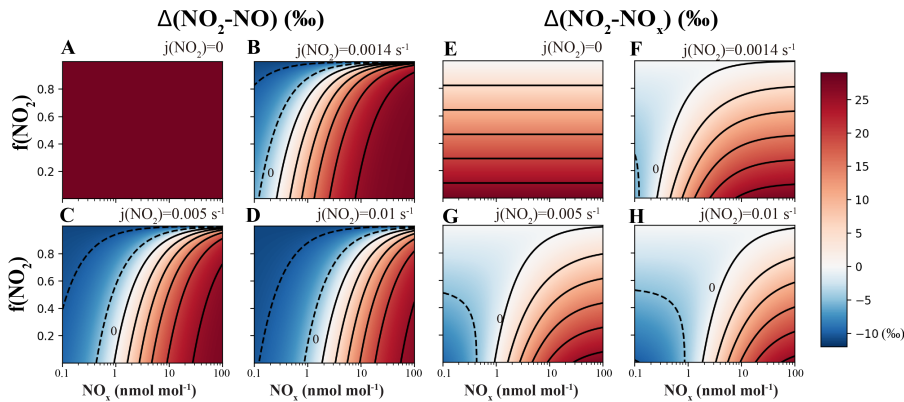
Deleted: black points

Deleted: red

Deleted:)

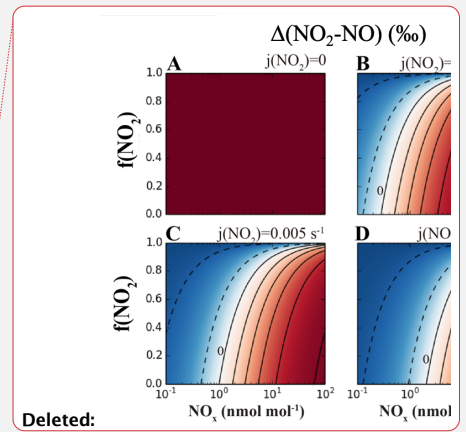
Deleted:)=

Deleted: observation

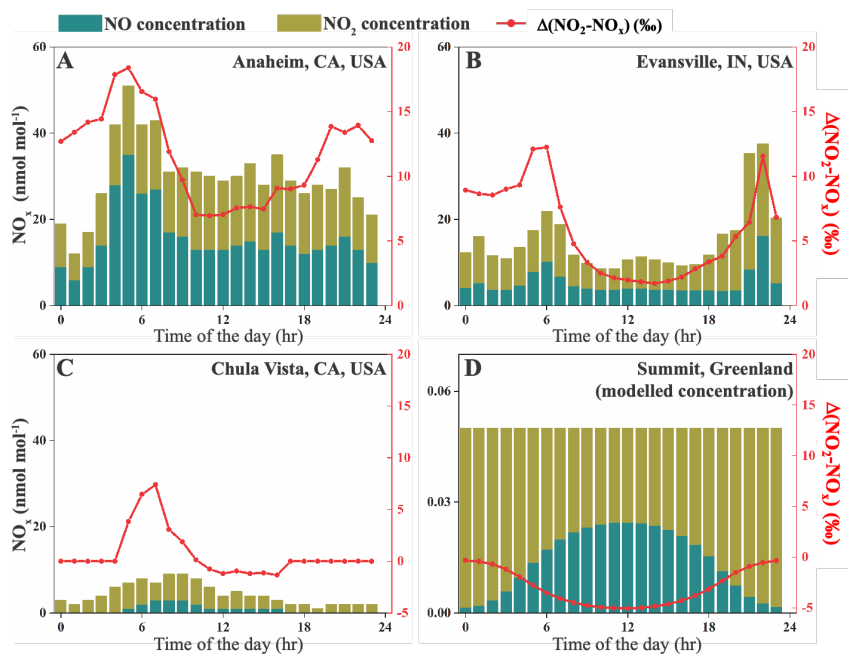


778

779 **Fig. 2** Calculating isotopic fractionation values between NO-NO₂ ($\Delta(\text{NO}_2\text{-NO})$, **A-D**) and NO_x-
 780 NO₂ ($\Delta(\text{NO}_2\text{-NO}_x)$, **E-H**) at various $j(\text{NO}_2)$, NO_x level and $f(\text{NO}_2)$ using Eq. (7) and (8). Each
 781 panel represents a fixed $j(\text{NO}_2)$ value (showing on the upper right side of each panel), and the
 782 fractionation values are shown by color. Lines are contours with the same fractionation values, at
 783 an interval of 5‰, the contour line representing 0‰ was marked on each panel except for A and
 784 E.



Deleted:



786
787
788
789
790
791

Fig. 3 NO_x concentrations and calculated $\Delta(\text{NO}_2-\text{NO}_x)$ values at four sites. Stacked bars show the NO and NO₂ concentrations extracted from monitoring sites (A-C) or calculated using 0-D box model (D); the red lines are $\Delta(\text{NO}_2-\text{NO}_x)$ values at each site. Note that the NO_x concentration (left-y) axis on panel D is different from the rest.

| Experiment | Number | NO conc. (ppb) | NO ₂ conc. (ppb) | O ₃ conc. (ppb) | $\delta(\text{NO}_2)$ (%) | f(NO ₂) |
|--------------------------------------|----------|-------------------|--------------------------------|-------------------------------|------------------------------|---------------------|
| Determining $\delta(\text{NO}_x)$ | <u>1</u> | <u>0.0</u> | <u>17.8</u> | <u>13.4</u> | <u>-59.5</u> | <u>1.00</u> |
| | <u>2</u> | <u>0.0</u> | <u>61.3</u> | <u>0.5</u> | <u>-58.9</u> | <u>1.00</u> |
| | <u>3</u> | <u>0.0</u> | <u>18.9</u> | <u>10.7</u> | <u>-58.0</u> | <u>1.00</u> |
| Dark experiments | <u>1</u> | <u>16.0</u> | <u>36.8</u> | <u>0.0</u> | <u>-51.8</u> | <u>0.70</u> |
| | <u>2</u> | <u>33.6</u> | <u>28.8</u> | <u>0.0</u> | <u>-43.9</u> | <u>0.46</u> |
| | <u>3</u> | <u>6.7</u> | <u>12.6</u> | <u>0.0</u> | <u>-49.6</u> | <u>0.65</u> |
| | <u>4</u> | <u>16.2</u> | <u>16.9</u> | <u>0.0</u> | <u>-45.1</u> | <u>0.51</u> |
| | <u>5</u> | <u>20.4</u> | <u>24.2</u> | <u>0.0</u> | <u>-46.8</u> | <u>0.54</u> |
| Irradiation experiments | <u>1</u> | <u>7.1</u> | <u>6.4</u> | <u>2.8</u> | <u>-47.5</u> | <u>0.47</u> |
| | <u>2</u> | <u>4.5</u> | <u>5.3</u> | <u>4.5</u> | <u>-48.7</u> | <u>0.54</u> |
| | <u>3</u> | <u>3.3</u> | <u>4.4</u> | <u>4.2</u> | <u>-49.8</u> | <u>0.57</u> |
| | <u>4</u> | <u>2.5</u> | <u>8.5</u> | <u>10.7</u> | <u>-54.6</u> | <u>0.77</u> |
| | <u>5</u> | <u>5.2</u> | <u>18.1</u> | <u>11.0</u> | <u>-54.0</u> | <u>0.78</u> |

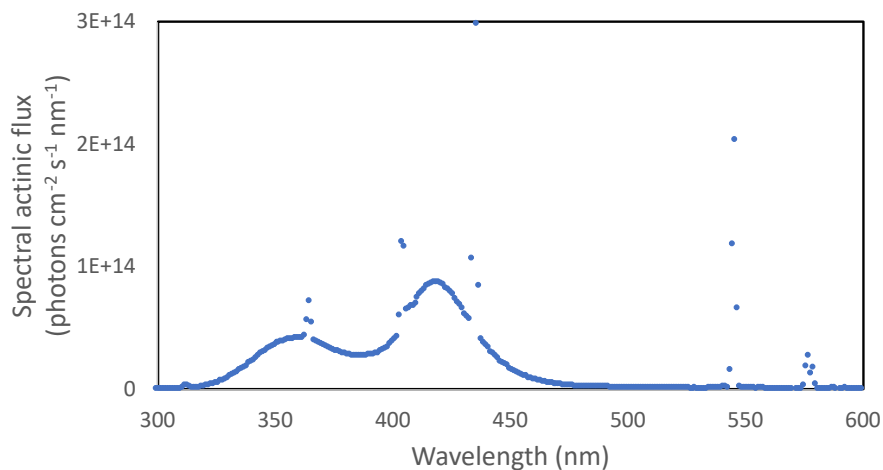
Table 1. Experimental conditions, concentrations of NO, NO₂ and O₃ at steady state, and measured $\delta(\text{NO}_2)$ values.

792
793
794

795 **Appendix A. Chamber descriptions**

796 The chamber is a 10 m³ Teflon bag equipped with several standard instruments including
797 temperature and humidity probe, NO_x monitor and O₃ monitor. 128 wall-mounted blacklight tubes
798 surrounded the chamber to mimic tropospheric photochemistry and the photolysis rate of NO₂
799 ($j(\text{NO}_2)$) when all lights are on have been previously determined to be $1.4 \times 10^{-3} \text{ s}^{-1}$, similar to a
800 $j(\text{NO}_2)$ coefficient at an 81-degree solar zenith angle. The irradiation spectrum of the blacklights
801 are shown in Figure A1. The chamber was kept at room temperature and one atmospheric pressure.
802 Before each experiment, the chamber was flushed with zero air at 40 L min⁻¹ for at least 12 hours
803 to ensure the background NO_x, O₃ and other trace gases were below detection limit.

804



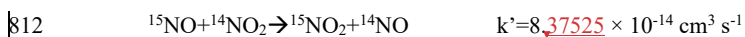
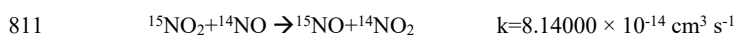
805

806 Figure A1 Spectral actinic flux versus wavelengths of the UV light source used in our experiments.

807

808 **Appendix B. Box model assessing the time needed for NO-NO₂ to reach isotopic equilibrium**

809 The time needed to reach NO-NO₂ isotopic equilibrium during light-off experiments were
810 assessed using a 0-D box model. This box model contains only two reactions:



813 Where k and k' are rate constants of the reactions. The differences in rate constants were calculated

814 by assuming an $\alpha(\text{NO}_2\text{-NO})$ value of 1.0289. Six simulations were conducted at various initial NO

815 (with $\delta^{15}\text{N} = 0\%$) and O₃ levels that were similar to our experiment. Then the $\delta^{15}\text{N}$ values of NO

816 and NO₂ during the simulation were calculated from the model and were shown in Figure B1,

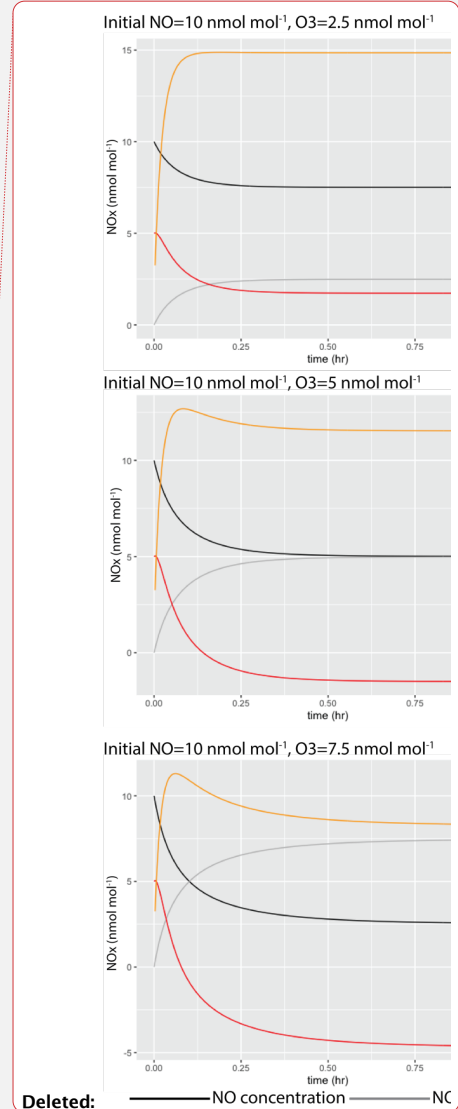
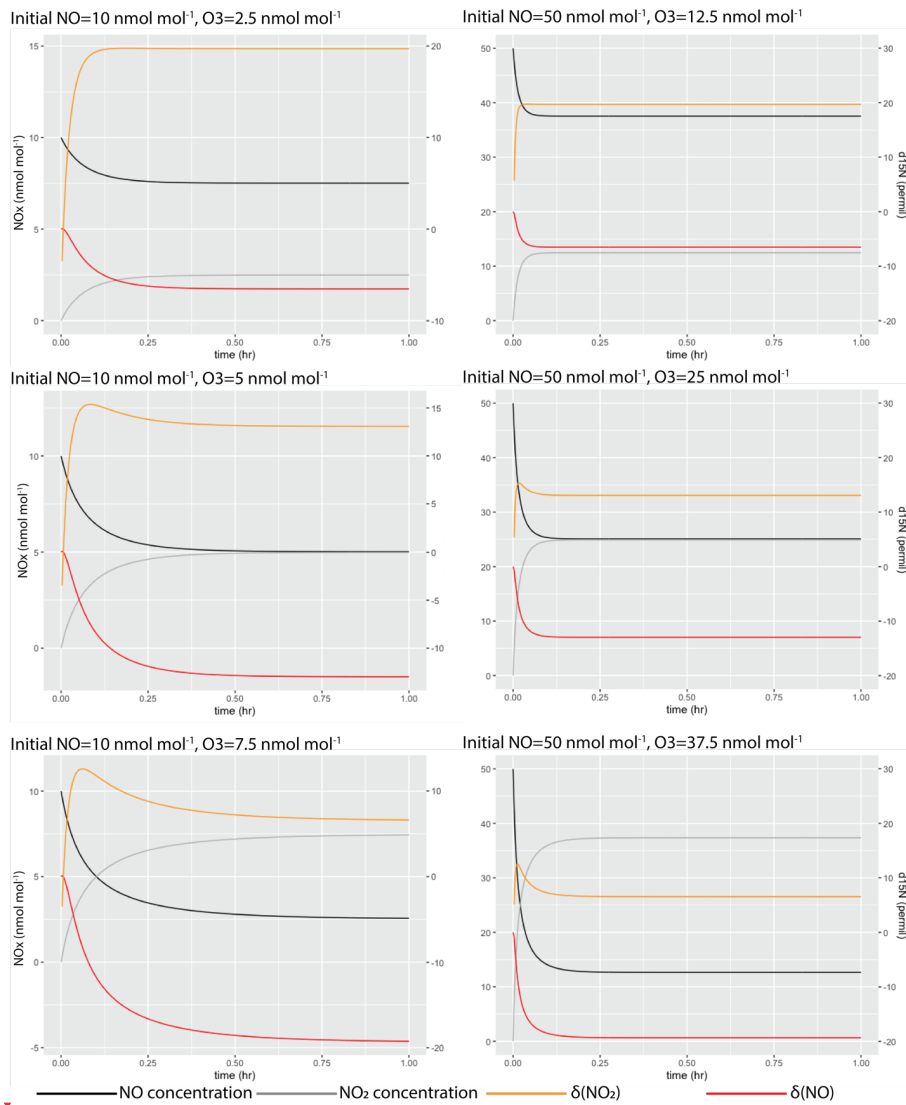
817 suggesting that in our experimental condition, all systems should reach isotopic equilibrium within

818 1 hr.

819

Deleted: 36385

Deleted: 0275



822

823 Figure B1 Simulated NO-NO₂ isotopic equilibrium process in the chamber at various NO and O₃
 824 concentrations.

Deleted:

826 **Appendix C. Deriving Equations 7 and 8**

827 When the system (R1-R6) reaches steady-state, we have:

828
$$d[^{15}\text{NO}_2]/dt=0 \quad \text{Eq. (C1)}$$

829 Therefore, using R1-R6:

830
$$k_1 [^{15}\text{NO}_2][^{14}\text{NO}] + j(\text{NO}_2)\alpha_1 [^{15}\text{NO}_2] =$$

831
$$k_5\alpha_2 [^{15}\text{NO}][\text{O}_3] + k_1\alpha(\text{NO}_2-\text{NO}) [^{15}\text{NO}][^{14}\text{NO}_2] \quad \text{Eq. (C2)}$$

832 From here we refer $^{14}\text{NO}_2$ and ^{14}NO as NO_2 and NO for convenience, rearrange the above equation,
833 we get:

834
$$\frac{[^{15}\text{NO}_2]}{[^{15}\text{NO}]} = \frac{k_5\alpha_2[\text{O}_3] + k_1\alpha(\text{NO}_2-\text{NO}) [\text{NO}_2]}{j_{\text{NO}_2}\alpha_1 + k_1[\text{NO}]} \quad \text{Eq. (C3)}$$

835 Meantime, since the Leighton cycle reaction still holds for the majority isotopes (NO and NO_2),
836 we have:

837
$$j_{\text{NO}_2}[\text{NO}_2] = k_5[\text{NO}][\text{O}_3] \quad \text{Eq. (C4)}$$

838 Thus,

839
$$\frac{[\text{NO}_2]}{[\text{NO}]} = \frac{k_5[\text{O}_3]}{j_{\text{NO}_2}} \quad \text{Eq. (C5)}$$

840 From the text, when $j_{\text{NO}_2} > 0$, we defined $A = \tau_{\text{exchange}}/\tau_{\text{photo}} = j_{\text{NO}_2}/(k_1 \times [\text{NO}])$. Using the above
841 equations, we know:

842
$$\frac{j_{\text{NO}_2}}{[\text{NO}]} = \frac{k_5[\text{O}_3]}{[\text{NO}_2]} = Ak_1 \quad \text{Eq. (C6)}$$

843
$$\frac{j_{\text{NO}_2}}{k_1[\text{NO}]} = \frac{k_5[\text{O}_3]}{k_1[\text{NO}_2]} = A \quad \text{Eq. (C7)}$$

844 Next, to calculate $\delta(\text{NO}_2) - \delta(\text{NO})$, we use the definition of delta notation:

845
$$\delta(\text{NO}_2) - \delta(\text{NO}) = R_{\text{NO}_2}/R_{\text{std}} - R_{\text{NO}}/R_{\text{std}} = (R_{\text{NO}_2}/R_{\text{NO}} - 1)(1 + \delta(\text{NO})) \quad \text{Eq. (C8)}$$

846

847
$$\frac{R_{NO_2}}{R_{NO}} = \frac{[^{15}NO_2][NO]}{[^{15}NO][NO_2]} = \frac{k_5\alpha_2[O_3][NO] + k_1\alpha(\text{NO}_2 - \text{NO})[NO_2][NO]}{j_{NO_2}\alpha_1[NO_2] + k_1[NO][NO_2]} \quad \text{Eq. (C9)}$$

848 Divide both side by $k_1[NO][NO_2]$:

849
$$\frac{R_{NO_2}}{R_{NO}} = \frac{\frac{k_5\alpha_2[O_3]}{k_1[NO_2]} + \alpha(\text{NO}_2 - \text{NO})}{\frac{j_{NO_2}\alpha_1}{k_1[NO]} + 1} \quad \text{Eq. (C10)}$$

850 Rearrange and substitute $\frac{k_5[O_3]}{k_1[NO_2]}$ and $\frac{j_{NO_2}}{k_1[NO]}$ with A:

851
$$\frac{R_{NO_2}}{R_{NO}} = \frac{\alpha_2 A + \alpha(\text{NO}_2 - \text{NO})}{\alpha_1 A + 1} \quad \text{Eq. (C11)}$$

852
$$\frac{R_{NO}}{R_{NO_2}} = \frac{\alpha_1 A + 1}{\alpha_2 A + \alpha(\text{NO}_2 - \text{NO})} \quad \text{Eq. (C12)}$$

853
$$\frac{R_{NO}}{R_{NO_2}} - 1 = \frac{(\alpha_1 - \alpha_2)A - (\alpha(\text{NO}_2 - \text{NO}) - 1)}{\alpha_1 A + \alpha(\text{NO}_2 - \text{NO})} \quad \text{Eq. (C13)}$$

854 Thus,

855
$$\delta(\text{NO}_2) - \delta(\text{NO}) = \frac{(\alpha_2 - \alpha_1)A + (\alpha(\text{NO}_2 - \text{NO}) - 1)}{\alpha_1 A + \alpha(\text{NO}_2 - \text{NO})} (1 + \delta(\text{NO}_2)) \quad \text{Eq. (C14)}$$

856 Then, using mass balance:

857
$$\delta(\text{NO}_2) f(\text{NO}_2) + \delta(\text{NO})(1 - f(\text{NO}_2)) = \delta(\text{NO}_x) \quad \text{Eq. (C15)}$$

858 We can derive Eq. 8:

859
$$\delta(\text{NO}_2) - \delta(\text{NO}_x) = \frac{(\alpha_2 - \alpha_1)A + \alpha(\text{NO}_2 - \text{NO}) - 1}{\alpha_1 A + \alpha(\text{NO}_2 - \text{NO})} (1 + \delta(\text{NO}_2)) (1 - f(\text{NO}_2)) \quad \text{Eq. (C16)}$$

Deleted: $\frac{\alpha_2 \times A + \alpha(\text{NO}_2 - \text{NO})}{\alpha_1 \times A + 1}$

Deleted: $\frac{R_{NO_2}}{R_{NO}} - 1 = \frac{(\alpha_2 - \alpha_1) \times A + (\alpha(\text{NO}_2 - \text{NO}) - 1)}{\alpha_1 \times A + 1}$

Formatted: Indent: Left: 2"

Moved (insertion) [3]

Formatted: Indent: Left: 1.5", First line: 0.5"

Deleted:

Moved up [3]: (C13)

Formatted: Indent: Left: 0", First line: 0"

Deleted: $\frac{(\alpha_2 - \alpha_1) \times A + (\alpha(\text{NO}_2 - \text{NO}) - 1)}{\alpha_1 \times A + 1} (1 + \delta(\text{NO}_2))$

Deleted: Since $\alpha_1 \approx 1$, $\alpha_1 \times A + 1 \approx 1 + A$ this equation can be further simplified to Eq. 7:

$$\delta(\text{NO}_2) - \delta(\text{NO}) = \frac{(\alpha_2 - \alpha_1) \times A + \alpha(\text{NO}_2 - \text{NO}) - 1}{A + 1} (1 + \delta(\text{NO}_2))$$

 → Eq.

Deleted: $\frac{(\alpha_2 - \alpha_1) \times A + \alpha(\text{NO}_2 - \text{NO}) - 1}{A + 1}$

Deleted: NO